The Synthesis of Solar Cell Dyes

Yasmeen Hameed

A Thesis Submitted to the Faculty of Graduate Studies in Partial Fulfillment of the Requirements

for the Master of Science

Graduate Program in Chemistry

York University

Toronto, Ontario

December 2013

Abstract

In the recent years, solar energy has become of great interest due to the diminishing supply of the fossil and nuclear fuels and their environmental effects. Solar energy is the most abundant and accessible renewable energy source, and this led the researchers to trend toward the dye-sensitized solar cell (DSSC). The dye-sensitized solar cell is the best technique to convert the solar light to different applicable types of energy such as electrical energy. Ruthenium-based dyes have been widely used in dye-sensitized solar cells.

The research proposal mainly focuses on an innovative approach to a new class of solar cell dyes, based on dicarboxylated terpyridine-type complexes. The research will focus on creating new ligands that will be used to attach the metal complexes, mainly Ru and Fe.

Acknowledgement

I especially would like to thank my supervisor Prof. Pierre G. Potvin for all his valuable advice and guidance. He inspired me greatly to work in this project. I am honored to work under his great supervision, and I am proud to be a part of his group.

I would also like to thank my committee members Prof. Sylvie Morin and Prof. Hongmei Zhu for their valuable time, constructive criticisms and cooperation. In addition, I would like to thank Dr. Howard Hunter for helping me in NMR data.

I would also like to thank my husband for his incredible help and support throughout my life, and I also would like to thank my family and my friends for their great support.

Finally, I would also like to thank York University for giving me such an opportunity to study at the Chemistry Department, and I would also like to thank Saudi Cultural Bureau for their supporting and funding.

Table of Contents

Index of Figures

List of Tables

List of Abbreviations

2D COSY	Two-Dimensional COrrelation SpectroscopY
2D HMBC	Heteronuclear Multiple Bond Correlation
2D HSQC	Heteronuclear Single Quantum Correlation
NOESY	Nuclear Overhauser effect spectroscopy
HOMO	Highest Occupied Molecular Orbital
LUMO	Lowest Unoccupied Molecular Orbital
DSSC	Dye-Sensitized Solar Cell
MLCT	Metal-to-Ligand Charge Transfer
CB	Conduction Band
ITO	Indium-Tin Oxide
FTO	Fluorine-doped Tin Oxide
TCO	Transparent Conductive Oxide
IR	InfraRed
UV	UltraViolet
NIR	Near-InfraRed
FT-IR	Fourier Transform InFrared

ESI-MS	ElectroSpray Ionization Mass Spectrometry
ISC	intersystem crossing
DMF	N,N’-dimethylformamide
NMR	Nuclear Magnetic Resonance
ppm	parts per million
s	singlet
d	doublet
dd	doublet of doublet
TMS	tetramethylsilane
TFA	trifluoroacetic acid
Ac	acetyl
Equiv.	equivalent
Et	ethyl
Bu	butyl
DCM	Dichloromethane
DBU	Diazabicycloundecene

1. Introduction

1.1. Dye-Sensitized Solar Cells (DSSCs)

Renewable energy sources will effectively replace fossil fuels which are the current primary energy resources. Solar energy is one of the most promising forms of renewable energy sources, and it is an ideal and great source of energy. The demand for energy is increasing these days, and there is an excessive use of non-renewable energy sources. According to recent studies, "the resource base represented by terrestrial irradiation exceeds by far that of all other renewable energy sources combined".[1] Harnessing this huge amount of the solar energy that falls on the earth is a good idea, especially because this solar energy is free and virtually limitless. The best idea to harness this solar energy is by converting the energy into more applicable forms by use of photosensitizers. A photovoltaic solar cell is the best means to utilize this renewable energy. Photovoltaic cells are able to convert the solar light to electrical energy. The Grätzel solar cell, also called dye-sensitized solar cell (DSSC), is a type of photovoltaic cell. It was invented by Michael Grätzel and Brian O'Regan in 1991, and it is considered as an alternative to traditional silicon-based solar cells. The efficiency of these photosensitizers requires improvement because it typically does not exceed 10-12%.[2]

There are many different types of solar cells such as the silicon solar cell, solid-state solar cell, organic solar cell, thin-film solar cell, thick-film solar cell, and dye-sensitized solar cell. These different types of solar cells are usually classified into three main categories called generations. The first generation of solar cells (silicon photovoltaic cells) is relatively expensive to produce, and it has a high efficiency. In addition, it is made of semiconducting p-n junctions. The second generation of solar cells (thin-film semiconductor) is relatively cheap to produce, and

it has lower efficiency than the first generation. The third generation of solar cells is a new generation which combines the advantages of the first and second generations. It is relatively cheap to produce, and it has a high efficiency.[3,4]

A silicon solar cell is the first generation of solar cells, and it represents 40% of the solar cell production. Crystalline silicon (c-Si) and amorphous silicon (a-Si) are the two types of silicon solar cells which are the most prevalent. The crystalline silicon solar cell can be classified into multiple categories depending on its crystallinity and its crystal size. These categories of crystalline silicon solar cell are monocrystalline silicon (single crystal silicon), polycrystalline silicon (multicrystalline silicon), and ribbon silicon. Moreover, this generation of solar cell is the traditional solar cell that has quite high efficiency and is very abundant. However, these silicon solar cells have a risk to lose some of their efficiency at high temperatures like hot sunny days. In addition, they need very pure silicon, and they are fairly expensive. Furthermore, they have a low band gap, and they are fragile. In comparison with amorphous silicon, crystalline silicon has a lower photon absorbance, and it has a smaller band gap. The band gap of the crystalline silicon is 1.1 eV while the band gap of amorphous silicon is 1.75 eV. However, the crystalline silicon has a higher efficiency than amorphous silicon, and it has a slower degradation over time than amorphous silicon. Generally, a lot of silicon solar cells are configured in n-p junctions (or vice versa) for one side and n^+-n-p^+ (or vice versa) for double sides, and all the contacts are in the back of the cell.[5]

A thin-film solar cell (TFSC), also called a thin-film photovoltaic cell (TFPV), is the second generation of solar cells, and it is made by depositing one or several thin layers of photovoltaic materials onto a substrate. The goal here is to produce solar panels at a lower cost,

and this is achieved by using less material in the manufacturing processes.[6] There are three main types of thin-film solar cells that can be categorized by the photovoltaic material that is deposited onto the substrate. These three types of thin-film solar cells are amorphous silicon (a-Si), cadmium telluride (CdTe), and copper indium gallium diselenide (CIGS).[7] This generation of solar cell requires a small amount of semiconductor material, and it is much cheaper to produce than crystalline silicon solar cells. Moreover, it has the best performance at high temperatures compared with other types of solar cells, and it has the best performance under low light conditions. In addition, it can be made flexible which can open up many new applications. However, it is very difficult to manufacture good films, and defective films will result in cells with low efficiency. Furthermore, these cells tend to degrade faster than crystalline silicon solar cell and require a lot of space.[6] In manufacturing these types of photovoltaic cells, health and environment can be affected by some chemical and physical hazards, such as the toxicity, corrosion and even explosion of materials. For example, the production of amorphous silicon requires hazardous gases, and cadmium is toxic.[8]

The third generation of solar cells is a new generation of solar cells that combines the advantages of the first and second generations. This generation of solar cells strives to achieve the highest efficiency of converting the light into electricity and to reduce the cost of solar cells.[9] The third generation of solar cells includes the dye sensitized solar cell (DSSC) and the organic solar cell (OPV). The new photovoltaic solar cell that is the DSSC is very different from the conventional silicon p-n type solar cell. A DSSC can offer both good performance with good stability and low cost. It requires low-cost materials and a low-cost manufacturing process. In addition, DSSCs have a special advantage; they are able to provide both cell flexibility and transparency. Moreover, they require a simple production process, and they use environmentally

benign materials in their manufacturing process. Thus, they have a low potential for environmental pollution and they have a good recyclability.[10,11,12,13]

1.2. The Structure and Operation of DSSCs

In fact, there are several types of DSSCs such as transition metal complexes (inorganic dyes) and pure organic dyes (metal-free organic dyes). These two types of dye sensitizers have very different structures. Polypyridyl metal complexes with Ru or Os are typical of inorganic dye sensitizers while organic dyes include natural and synthetic organic dyes.[14] The transition metal complexes have relatively higher power conversion efficiencies than pure organic dyes. The Grätzel cells using Ru dye complexes are the best known type of DSSC because of their high efficiency. However, pure organic dyes have many advantages compared to inorganic dyes for their application in DSSCs, such as their large absorption coefficient, their low cost and their wide diversity of molecular structure due to their easy modification in the molecular design.[15,16,17]

The design of the Grätzel cell as shown in Figure 1 consists of three parts that are a photo-electrode, an electrolyte (solid-state or liquid) and a counter-electrode. In addition, it also involves a set of different layers that include a transparent conducting layer, nanocrystalline TiO_2, and dyes. The photo-electrode and the counter-electrode are built onto transparent glass plates. In dye-sensitized solar cells, the glass substrate is not the only choice; it can be any surface that is strong enough to support these layers such as plastic.[18,19]

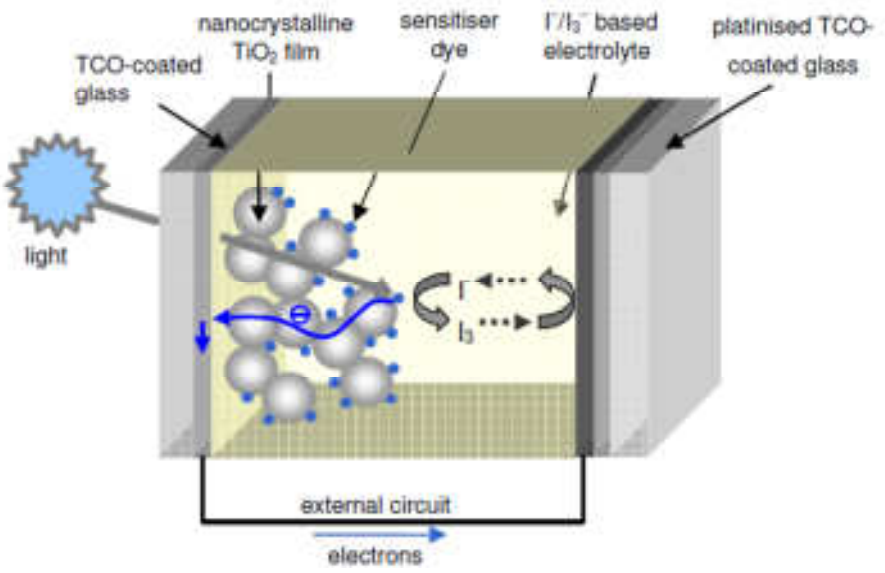

Figure 1. Schematic of a liquid electrolyte dye-sensitized cell (taken from reference 20).

The glass substrate is usually coated with indium-tin oxide (ITO), a transparent conductive oxide (TCO) that acts as the contact. Fluorine-doped tin oxide (FTO) glass is another common transparent conductive oxide (TCO) that has been widely used for the DSSC. The glass is then coated with a film of semiconducting titanium dioxide particles TiO_2 (anatase), which is then covered with a film of ruthenium polypyridyl complexes as photosensitizer.[18,20, 21,22]

Ruthenium-based dyes have been widely used in photovoltaic cells due to their strong, wide absorptions over much of the visible range as well as the ultraviolet region, moderately long excitation lifetime, and efficient metal-to-ligand charge transfer.[18,20]

In addition, the nanocrystalline titanium dioxide (TiO_2) became the semiconductor of choice for the photoelectrode because it has a high structural stability under solar irradiation, low cost, and wide availability. Moreover, it is environmentally benign because it is non-toxic, and it is also very abundant.[18,23,24]

The nanocrystalline TiO_2 is made of fused spheres and that leads to high porosity. This is very important because it provides two advantages: first, it offers very large surface area to attach the dye molecule. The dye molecule can penetrate into the surface through the porosity and it will attach to much of the surface of TiO_2. Secondly, the electrolyte can penetrate within the pores at the same time in order to perform its function.[25,26,27]

There are two different crystal structures of titanium dioxide, anatase (a-TiO_2) and rutile (r-TiO_2). The anatase phase (a-TiO_2) is most popular, and the most work on DSSCs has been focused on the anatase form of TiO_2. This anatase phase (a-TiO_2) gained this important property for the DSSCs due to its large active surface chemistry and to its small particles that leads to an increase in dye adsorption. Compared with the anatase-based solar cell, the rutile-based solar cell has slower electron transport in the rutile layer than in the anatase layer. This difference is because of the differences in the extent of the connectivity between the particles associated with the packing density of particles.[28,29,30,31]

The other glass plate, the counter-electrode, which is on the back of the DSSC is coated with an electrocatalyst usually made of a layer of platinum, and this thin layer of platinum acts as the cathode to regenerate I^-.[18,20,22]

Figure 2 shows the catalytic cycle during the cell operation. This catalytic cycle illustrates how the iodide/triiodide redox couple is in equilibrium, and how an electron transfers from the dye-based ground state to an excited state of the dye.[20,32]

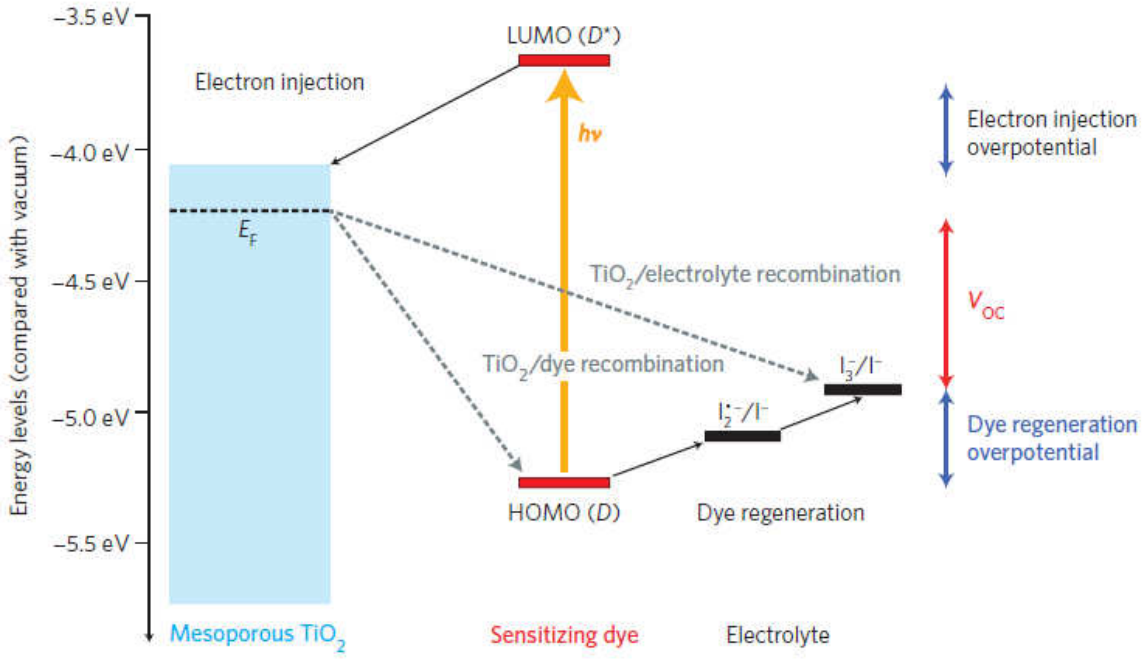

Figure 2. The dye sensitized solar cell operation (taken from reference 42)**.**

When light comes through the uncoated back side of the photo-electrode and hits the dye surface, it is absorbed by a monomolecular layer of dye on the coated side. This absorption promotes an electron from the Ru^{II}-based ground state to an excited state (Ru^{II*}) (equation 1), and there is a metal to ligand charge transfer. The excited electron is injected into the conduction band of the TiO_2 surface, leaving behind the oxidized form of the photosensitizer (Ru^{III}) (equation 2).[18,32,33,34]

$$D + h\nu \rightarrow D^{*} \qquad (1)$$

$$D^{*} \rightarrow D^{+} + e^{-} (TiO_2) \qquad (2)$$

$$I_3^{-} + 2\, e^{-} \rightarrow 3\, I^{-} \qquad (3)$$

$$2D^{+} + 3\, I^{-} \rightarrow 2D + I_3^{-} \qquad (4)$$

The injected electron in the conduction band of TiO_2 transfers to the TCO, and then the electron reaches the counter electrode after passing through the circuit. At the counter-electrode, the electron reduces I_2/I_3^- to I^- (equation 3). The I^- travels back to the photo-electrode and reduces the oxidized photosensitizer (Ru^{III}) leading to regeneration of the dye ground state (Ru^{II}) (equation 4). In the electrolyte, the oxidized redox mediator (I_3^-) diffuses back to the counter electrode, and the cycle can start again.[18,32,33,34]

The two electrodes are placed in an electrolyte containing a high concentration of the iodide/triiodide (I^-/I_3^-) redox couple in an organic solvent such as acetonitrile or methoxyacetonitrile. This is the most common electrolyte, and this kind of electrolyte is good for ion diffusion and infiltrates well within the TiO_2 film, promoting the highest efficiency of all DSSCs. In addition, this combination leads to the highest efficiency known.[18,20]

However, this electrolyte and these solvents have problems in terms of long-term stability because solvents tend to leak and evaporate, even if the cell is hermetically sealed. Our experimental cells use acetonitrile because we only want to test their efficiency.[35,36]

However, it is clear that the iodide/triiodide (I^-/I_3^-) redox couple is not the ideal redox couple because it has some problems. For example, I^-/I_3^- absorbs visible light, and this may reduce the amount of light that is available to the dye. In a DSSC, the light comes in from the back of photo-electrode and hits the dye surface first. Any light that passes through will continue through the electrolyte onto the platinum surface on the other electrode and reflect back toward the dye, so that the dye has a second chance to intercept a photon. However, because the iodide/triiodide redox couple is coloured (brownish red) and absorbs a lot of the visible light,

there is less light reflected by the platinum surface, and there is less light reaching the dye layer that there could be.[37,38,39]

Another problem is corrosion of the circuit contacts. In a DSSC experimental cell, the most common way of joining copper wire to the TCO is through ordinary alligator clips. In an installed cell, a soldered contact would be used. The problem with iodide/triiodide is that when it leaks, it tends to cause corrosion towards most metals such as silver, copper, aluminium, and gold. This corrosion weakens the connectivity of the joint, and therefore it is not good for the circuit. This then requires extra protection of the metal parts, and this will increase the manufacturing costs.[38,39,40,41]

Another disadvantage of the I^-/I_3^- system is that the iodide/triiodide redox couple has a relatively low redox potential, and this limits the open-circuit voltage (V_{OC}). To improve the efficiency, the redox potential of the electrolyte needs to be as positive as possible to increase V_{OC}.[35,38,42,43]

On the other hand, there are alternative redox couples. There are two basic categories of these alternative redox couples, molecular species and transition-metal-based complexes.[38,44] Many varieties of molecular species have been studied to replace the iodide/triiodide such as $SCN^-/(SCN)^{3-}$, $SeCN^-/(SeCN)^{3-}$, Br^-/Br^{3-}, and hydroquinone.[38,44] As well, a wide variety of the transition-metal based complexes have been studied as alternative redox couples such as cobalt(II/III), copper(I/II), nickel(III/IV), ferrocene/ferrocenium(Fc/Fc^+) complexes.[35,38,42,44,45]

Cobalt ($Co^{II/III}$) polypyridine complexes have drawn attention because they present some important advantages such as their low visible-light absorption, their low corrosiveness, and their

positively high redox potential, which leads to an increase on the open-circuit voltage (V_{OC}).[40,42,43]

However, the overall conversion efficiencies with these alternative redox couples do not outperform the conversion efficiency with iodide/triiodide. The photovoltaic performance with the alternative redox couples is affected by several factors, such as fast electron recombination and the slow dye regeneration.[43,44,46] Nevertheless, our experiments use the iodide/triiodide system because we want to compare it with the standard that we adopted, which is N3 dye. N3 dye shows a high conversion efficiency (11%) in combination with I^-/I_3^-.[47,48,49,50]

Many attempts have been made to replace liquid electrolytes with solid-state or quasi-solid-state electrolytes. This offers several advantages in terms of size, weight, and flexibility. The most important advantages of the solid-state and quasi-solid-state electrolytes are a high long-term stability, no corrosiveness and no solvents to leak or dry up.[35,36,51]

1.3. The Design of DSSCs

The design of the DSSCs has to meet some requirements in order to obtain a high efficiency. For example, the redox mediator's oxidation potential must be higher than the dye's ground-state oxidation potential in order to accept electrons effectively and to be able to regenerate the dye after photo-excitation of electron injection.[52,53,54,55]

Another requirement is that the excited state level of the dye must be a little higher in energy than the conduction band (CB) of the semiconductor in order to inject the electron efficiently.[52,53,54]

The voltage output of the DSSC is determined by the difference between the redox potential of the redox couple in the electrolyte and the conduction band of TiO_2.[53,54]

In meta- based dyes, the band gap is the difference between the unrelaxed excited state energy and the ground- state energy, is related to the wavelength absorbed. Thus, the HOMO-LUMO gap needs to be suitable to absorb light in the visible region while leading to a sufficiently high-energy excited state.[56]

Although much of solar light is the visible light, and there is also near-infrared light (NIR). Some of the solar irradiance lies in the NIR region, and this is largely not absorbed by dyes. Those are relatively low energy wavelengths, and the absorption of the dye should ideally be extended to the NIR. There have been several attempts to generate a dye that is able to absorb strongly in the NIR, which means that the minimum HOMO-LUMO needs to correspond to those kind of wavelengths (900 -1200 nm). However, then dye will also be able to absorb longer wavelengths as well, and those will then send the electrons to much higher orbitals.[20,50,57,58,59] Fortunately, intersystem crossing brings down the electron from the very high-energy LUMOs to the lowest-energy excited state LUMO which then can transfer it to the CB. However, that represents a loss of energy because it is not used to generate the cell voltage. Consequently, that energy becomes heat, and the cell tends to warm up. We do not want the cell to be operating at a temperature that accelerates the decomposition of the cell, leaking the solvents or changing the photovoltaic parameters. A low HOMO-LUMO gap means a high-lying HOMO, since the LUMO needs to lie above the CB. This limits the redox range of the redox mediator and cuts down the V_{OC}. [20,50,57,59]

The dye should also carry attachment groups such as carboxyl groups to be able to graft itself onto the semiconductor oxide surface. To inject the electrons into the solid efficiently after the excitation, there ideally should be good orbital overlap between the CB and the excited state.[20,60]

With Ru(II) dyes, the optical transition has MLCT (metal-to-ligand charge transfer) character, that is excitation of the dye promotes an electron from the metal-based HOMO to a π^* orbital of the ligand, leads to charge separation.[20]

The dye itself needs to be photo stable and thermo stable. [61,62,63,64] For instance, in the case of bipyridine complexes, such as N3, the absorption of light sometimes results in ejection of a pyridine nitrogen that opens up a coordination site around the Ru that the solvent can then occupy. The nitrogen may come back at room temperature, albeit slowly. That process is called anation. Moreover, bipyridine can do this more than once, and an entire bipyridine molecule can be lost from the complex. The bipyridine complexes are quite stable but terpyridine complexes are much more stable, so a high degree of chelation is very important.[65,66,67,68]

In addition, N3 has unidentate thiocyanate groups that usually link through the nitrogen atom. Such unidentate groups are much more easily lost by both thermal and photochemical process.[68]

The absorption rates are very fast, on the order of 10^{11} s^{-1}, and intersystem crossing (ISC) is also fast (92 fs). The transfer to the conduction band is also on the femtosecond time scale.[20,69] In view of this, the excited state lifetime (typically on a nanosecond time scale) is less important than it would be in homogeneous solution. Normally, the lifetime of the exited state in Ru complex is in the nanosecond range, whereas some other complexes show excited state lifetimes

measured in the microsecond or millisecond ranges. However, that is still good enough because they transfer the excited electron into the conduction band in femtosecond, so this step is much faster. Thus, the exited state lifetime is not a critical component.[70]

There is a back reaction that can affect the DSSC performance, and this is a return of the injected electron from the conduction band to the ground state of the dye. There is also non-radiative loss, where the exited state just returns back to the ground state, and the energy is dissipated as heat.[70,71]

One other important side reaction is recombination. Recombination is when the injected electron is transferred directly to the oxidized form of the redox mediator. That means that if a triiodide has access to the TiO_2, it can pick up the electron and generate iodide. That iodide can then reduce the oxidized dye and return it back to the ground state. Thus, using light to promote the electron, transfer it to the conduction band, to the redox mediator and then return it back to the oxidized dye basically short-circuits the cell. These three important side reactions are considered wasteful of the energy, and they reduce the conversion efficiency. Thus, they lead to reduce DSSCs performance. [20,42,72,73]

As previously mentioned, triiodide can penetrate through the pores of the titanium dioxide surface, where it could promote this short-circuiting recombination. This can be reduced by limiting access to the surface with very high dye loadings, or with an additive to cover the surface of the TiO_2 that does not contain dye. Some examples of additives are 4-tert-butylpyridine (TBP) and cholic acid. 4-Tert-butylpyridine has been widely used as an additive. Cholic acid is a steroid with three hydroxy groups, and it will bind very strongly to TiO_2.[20,42,60]

1.4. The Photovoltaic Efficiencies of Grätzel Cells

The best photovoltaic efficiencies in terms of conversion yield and long-term stability have been achieved with polypyridyl ruthenium(II) complexes. N3 dye, N719 dye, and black dye are the most well-known Ru complexes showing the highest efficiencies in DSSCs and constitute benchmark reference dyes. Black dye has a superior photovoltaic efficiency.[14,74]

As shown in Figure 3, N3 and N719 have the general structure ML_2X_2 where M represents the metal, L represents the ligand 2,2'-bipyridyl-4,4'-dicarboxylic acid, and X or X_2 represents an ancillary ligand such as a halide, cyanide, thiocyanate, or acetylacetonate. Moreover, N719 dye is simply a particular salt of the N3 dye, with $^{n}Bu_4N^{+}$. On the other hand, black dye has the general structure MLX_3 where M represents the metal Ru(II), L represents the ligand 2,2';6';2''-terpyridyl-4,4',4''-tricarboxylate, and X represents an ancillary ligand, thiocyanato (NCS^{-}).[14,74]

Both N3 and N719 have local symmetry in the sense that all four pyridine rings are normally the same from the electronic point view. There are some slight differences between those trans to each other and those that are not. In addition, all three dyes in Figure 3 are attached to the titanium dioxide surface through just two carboxylic groups. Occasionally, a third will be used depending on whether or not dye is seated in a pocket, and is able to reach a second surface. However, most often only two carboxylic groups are used. In any case, there have been some suggestions that those groups that are not used for binding can actually be detrimental.[20,71,75]

Black dye has some symmetry. The central pyridine is different from the other two, but the other two are the same. However, as soon as it binds using two adjacent carboxylic groups, the third one becomes different. This produces slight differences in the energy levels and among

orbitals over the three pyridine rings. Such slight differences broaden the absorption envelopes.[20,75]

Halide, cyanide, thiocyanate and several other ancillary groups have been tested in N3 and black dye, and it turns out that the thiocyanates are the best in this family. The reason seems to be that it facilitates the reduction of the oxidized version of the dye by iodide, and that seems to require interaction with the sulfur orbitals. Those kinds of interaction are simply not available with the other groups.[20,76,77]

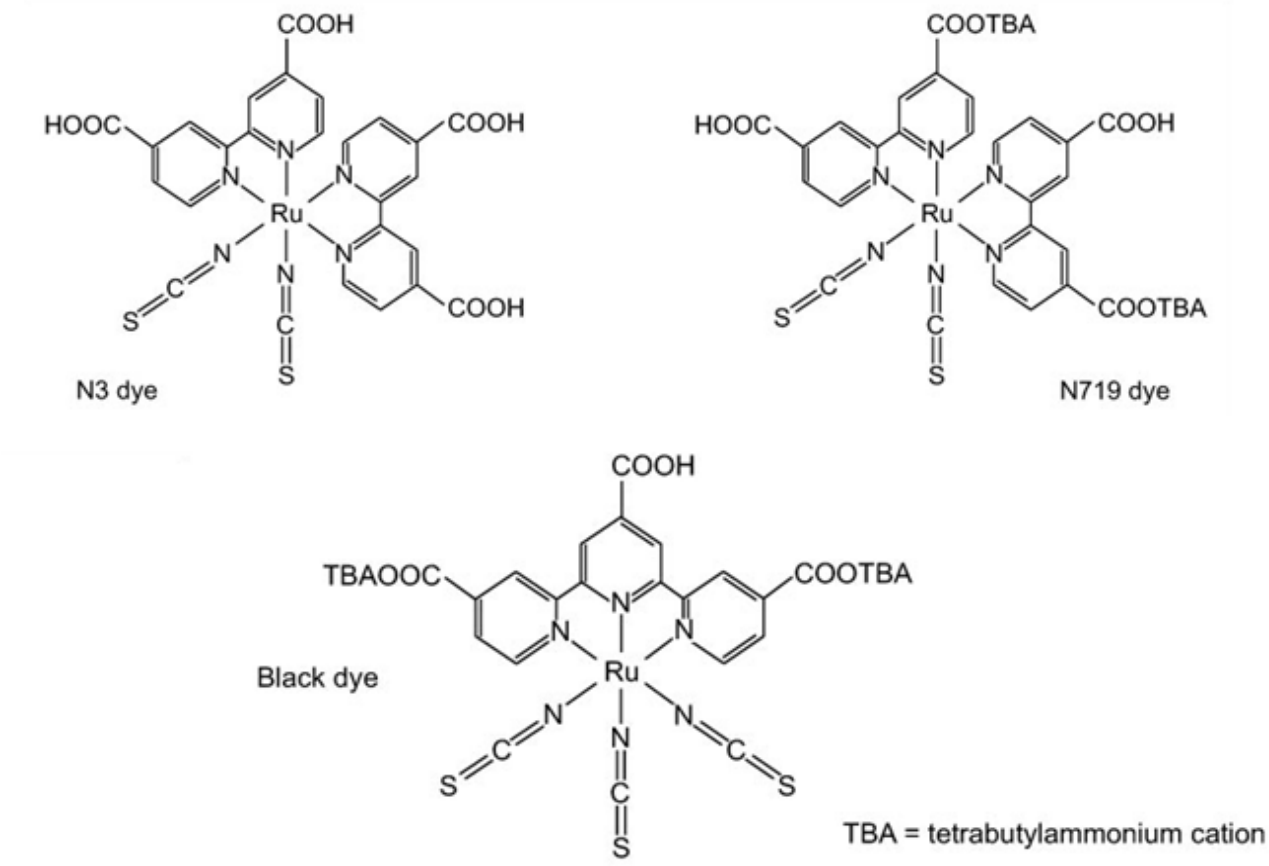

Figure 3. Structures of N3, N719 and Black dyes, the most efficient DSSC dyes (taken from reference 74).

1.5. Iron Complexes[75,78,79,80,81,82]

In 1998, Ferrere and Gregg reported iron(II) polypyridyl chromophores that can replace ruthenium(II) polypyridyl chromophores in the DSSC applications. Iron(II) polypyridyl chromophores are currently of great interest due to their low cost, their abundance, and their recyclable metal. This promising result led us to focus in our research to prepare iron(II)-based chromophores.

Although many of the first row transition metals are more abundant and cheaper than ruthenium, iron is the best choice in replacing ruthenium because it shares several similar properties.

As previously mentioned, the excited state of a chromophore should be higher than the conduction band of TiO_2, and it should be sufficiently long-lived for an electron to be injected into the conduction band of the TiO_2 semiconductor before relaxing to a lower ground state. This means that the injection from an upper lying excited state into the semiconductor prior to any relaxation would be required. However, it has been reported that iron(II) based complexes have extremely short-lived charge transfer excited states.

Several attempts have been made to determine the deactivating coordinate of the MLCT excited state and to study the relaxation dynamics of potential sensitizers. A series of iron(II) terpyridyl complexes has been prepared to investigate the steric effects on rotational freedom about the C2 axis that may modulate MLCT to the ligand field kinetics. There is a suggestion that torsional twisting modes can be involved in the relaxation from the initial excited state to the longer-lived ligand field excited state.

In addition, the iron(II) sensitizer with a low-spin ground state have better metal-ligand orbital overlap than a high-spin complex. This results in an increase in metal-ligand bond length because it provides good electronic communication between the metal and the ligand which increases the intensity of the MLCT. Moreover, iron(II) low spin complexes are more stable than high spin complexes that are more easily oxidized to iron(III) in air, and that will affect the long term stability in a DSSC.

Iron complexes that have different ligands are called mixed-ligand complexes. The preparation of well-defined mixed-ligand iron complexes is very difficult because they tend to undergo scramble ligand which means that the ligands exchange rapidly between the complexes. For instance, if we have 1:1 ratio of terpyridine with an ordinary iron salt, then we will have a mixture of complexes in solution consisting of the 1:1 complex, the 2:1 homoleptic complex and free iron. The absence of well-defined species is a common difficulty. Cyano-containing Fe complexes, such as Ferrer's, are exceptions.

Our approach is twofold. First, we are going to assemble mixed ligand Fe(II) complexes on the surface of titanium dioxide TiO_2. Basically, the idea is to attach the ligand to the surface first, and then to introduce the iron. This will prevent ligand scrambling. The second approach is to use homoleptic complexes, which are easy to prepare.

1.6. The Proposal

This project mainly focuses on an innovative approach to prepare a new class of solar cell dyes, based on dicarboxylated terpyridine-type complexes. The research will focus on creating new ligands that will be used to attach Ru and Fe.

The first design (**C_A**) in Figure 4 has the general formula of $[MLX_3]^-$, with L representing a terpyridine-based ligand with three anchoring groups (consisting of two carboxylic acid groups and one 2-furylmethanol group). This design still has an element of symmetry like the black dye, but we get a slight change of symmetry once it is surface-bound through two of the three anchoring groups. However, the difference from the black dye is the furyl methanol group that is considered a relatively strong binding group. The furan ring is relatively π-electron rich. Moreover, the alkoxy oxygen is not π-connected to the furan ring and therefore disconnected from the terpyridine ring. Thus, this group is simply an anchoring group and the furan ring serves as an electron-donating group. The furan tends to raise the LUMO levels for those orbitals centered over the central ring. It reduces the electron deficiency in the central pyridine ring, compared to what that in black dye, which makes the outer rings relatively electron-poor, which is where we want the excited state electron density to lie, where the π-connected carboxy is located. This design is simple to make, but it does suffer from the same potential drawback as black dye. This potential drawback is that there will be one unused carboxylic acid group that may affect performance. As previously mentioned, unused carboxylic acid groups have been shown to be problematic.

The second dye design (**C_B**) has the general formula of $[MLX_3]^-$ where M is the metal, L is the terpyridine based ligand with two carboxylic acid anchoring groups, and X are

isothiocyanate groups. The terpyridine-based ligand bearing two carboxy groups are destined to be the electron-poor portions of the ligand. The three isothiocyanate groups are relatively electron-rich and will supply electron density distally. This is a variant of black dye which lacks its third carboxylic group. Thus, presumably we can avoid the problem of unused carboxylic group. This design is more asymmetric, which gives different LUMO levels and a broader absorption envelope.

The third design (**C_D**) is a homoleptic complex that has the general formula of $[ML_2]^{2+}$. The ligand L is a tridentate with a single carboxylic group, an electron-donating group at the central ring and potentially an electron-donating third ring, such as phenylene. This clearly has no local symmetry, and can have two sources of electron donation, making very different ligand orbital levels. The electron donating group could be an aniline type, anisole, pyrrole or similar type. The idea is not so much to push electron density towards the anchoring groups but to force the excited-state electron into those orbitals centered nearest the anchoring groups.

With a phenylene third ring, the complexes will be part of class of complexes called cyclometalated complexes, and there are numerous examples of these. These complexes show differences in the spectral properties and in the electrochemical properties. With an ionic ligand, the LUMO levels are raised, and the HOMO levels driven even higher, which then raises the HOMO-LUMO manifold relative to the conduction band, and relative to the iodide/triiodide redox couple. The HOMO-LUMO gap narrows whenever there is an electron-donating group or electron-withdrawing group. The narrowing of HOMO-LUMO gap means that the lowest energy absorption will be at longer wavelength, reaching toward the red and NIR regions. We also expect to see a very broad absorption due to the low symmetry.

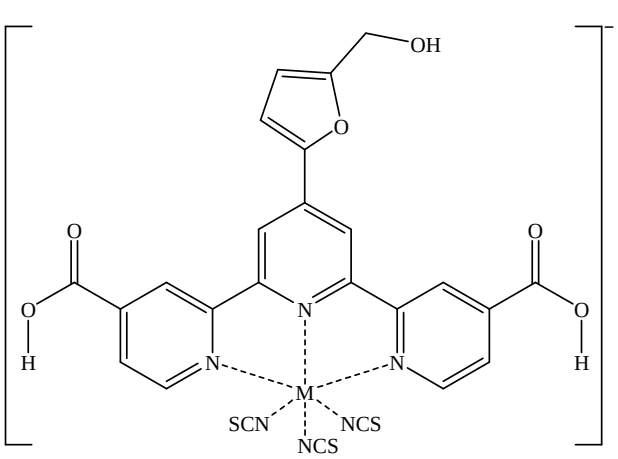

C_A

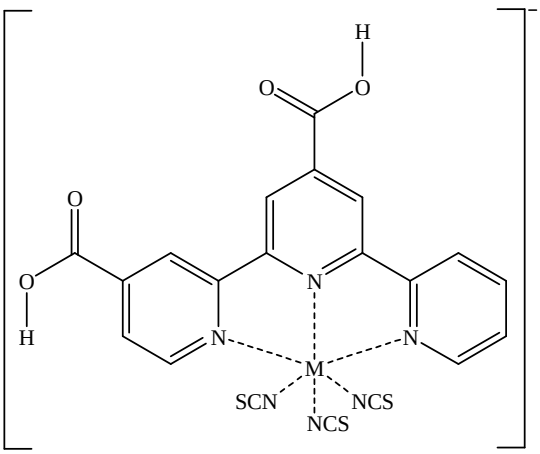

C_B

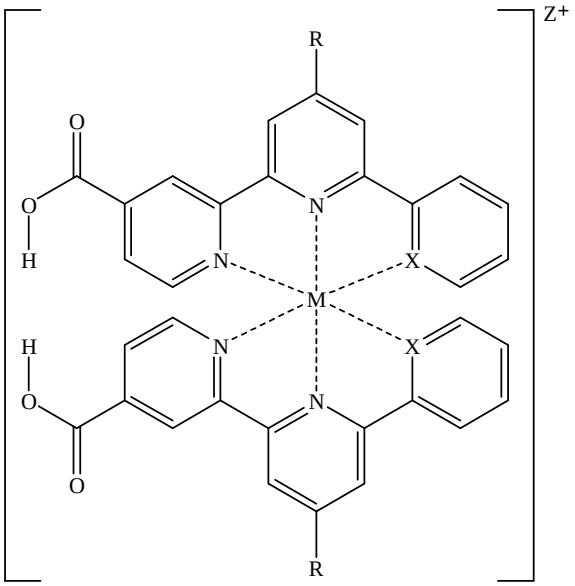

C_D

M = Ru or Fe

X = N or C

Z = 2 or 0

Z = 2 when **X** = N**, Z** = 0 when **X** = C

R = Electron Donating Group

Figure 4. The structures of the dye designs.

2. Experimental Section

2.1. Materials & Instruments

The reagents that used in the experiments were purchased from Sigma-Aldrich and Alfa Aesar, and all the solvents used were from Caledon Labs Inc. NMR spectroscopic data were acquired using Bruker ARX (AV) 300, 400, and 600 MHz spectrometers. ESI-MS data were obtained using a QSTAR Elite Quadrupole-TOF instrument. FT-IR spectroscopy was performed using a Nicolet 380 FT-IR Spectrophotometer. UV-visible analysis was obtained using a Ultrospec 4300 Pro UV/Visible Spectrophotometer.

There are some known compounds such as **P7** and **P8** that are involved in the synthesis of some ligands.

The production of the pyridinium salt **P7** (Figure 5) is mentioned in the literature.[83]

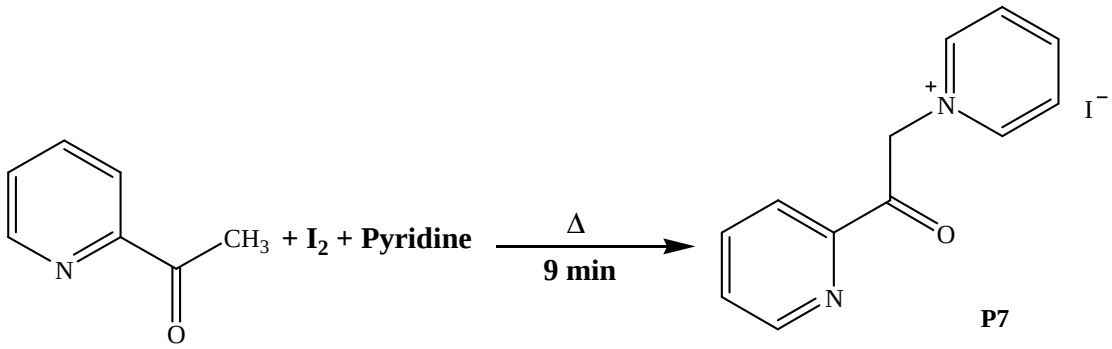

Figure 5. The synthesis of pyridinium salt **P7.**

The production of this enone **P8** is mentioned in the literature procedure,[84] and Figure 6 illustrates the synthesis of this enone **P8**.

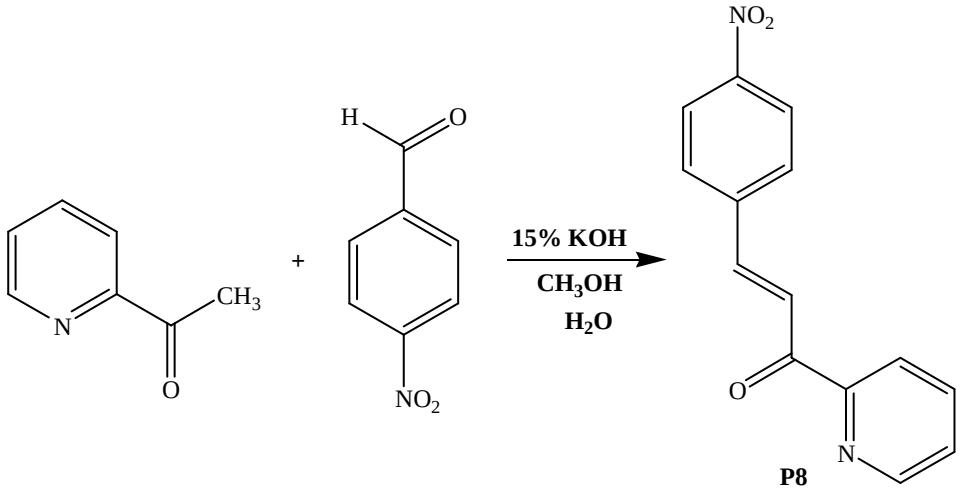

Figure 6. The synthesis of enone **P8**.

2.2. Compound P1 (Minisci Compound/Methyl 2-Acetylisonicotinate)

Compound **P1** was prepared using the procedure[83] illustrated in Figure 7. Methyl isonicotinate (1.02 mL, 8.6043 mmol) was mixed with paraldehyde (> 97%, 6.8 mL, 51.144 mmol) in a round bottom flask containing 3 mL tBuOOH (70%), 0.66 mL TFA (8.6 mmol), 25 mL CH_3CN, and $FeSO_4.7H_2O$ (0.05 g, 0.1798 mmol). The flask was equipped with a stirring bar, and the mixture was heated to reflux for two hours. The reaction mixture was then evaporated, and extracted twice with toluene. The toluene layers were collected and evaporated. The product was a brown solid with a mass of 1.4376 g, which corresponds to a 93% yield. The NMR data, the data match those in the literature.[83]

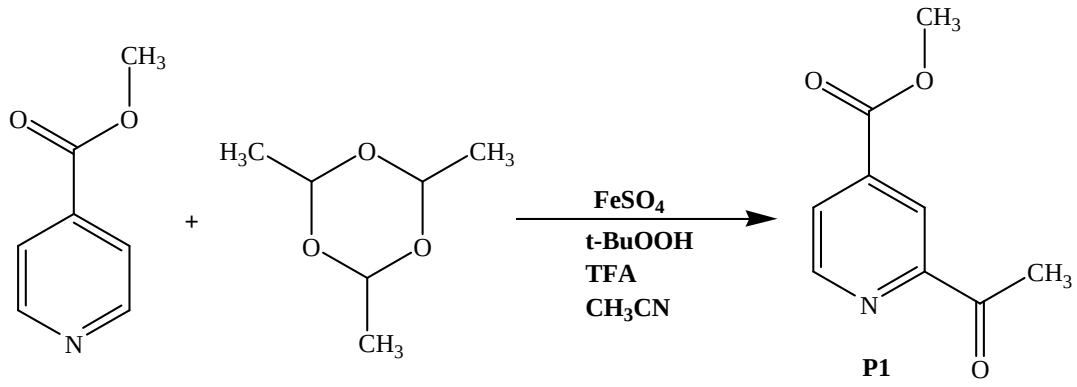

Figure 7. The scheme of compound **P1**.

2.3. Compound P6 (1-(2-(4-Methylcarboxyl)pyridinyl)carbonylpyridinium Iodide)

Compound **P6** was prepared by following the procedure that was reported in the literature,[84] and Figure 8 illustrates the synthesis. A mixture of compound **P1** (0.2388 g, 1.3346 mmol), I_2 (0.3387 g, 1.3346 mmol), and pyridine (10.0 mL) was boiled for 9 minutes. The mixture was allowed to cool to room temperature and left for many days to precipitate. The solid was isolated by filtration and washed with $CHCl_3$, yielding the product as a brown solid (0.2865 g, 55%). The spectral data matched those in the literature.[83,85]

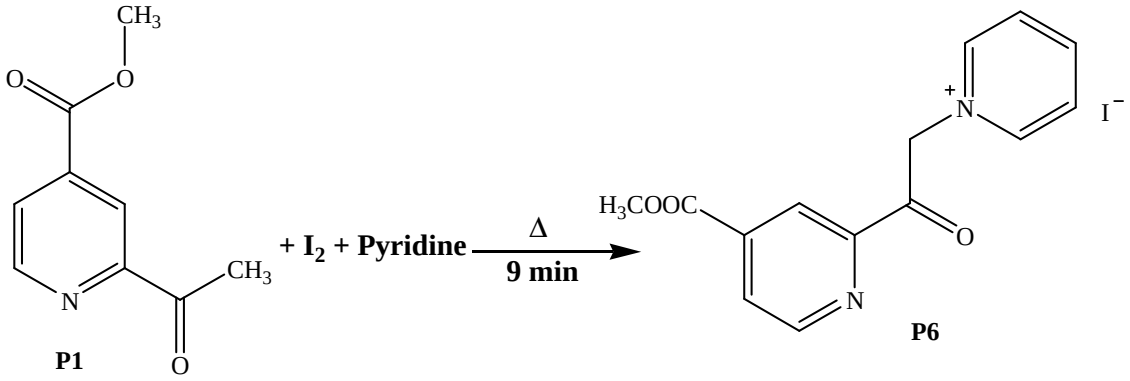

Figure 8. The scheme of compound **P6**.

2.4. Compound P11

Minisci product **P1** (0.3197 g, 1.7863 mmol) and furfural (0.15 mL, 1.7863 mmol) were mixed with an excess of K_2CO_3 (0.5 g) and dissolved in MeOH (10 mL), as is illustrated in Figure 9. The product precipitated out of the reaction mixture after 10 minutes at room temperature. The mass of the product was 0.1568 g corresponding to a 34% yield. The melting point was 140-241° C. ^{1}H-NMR (300 MHz, $CDCl_3$): δ 8.95 (d, J = 4.8 Hz,1H), 8.71 (s, 1H), 8.19 (s,1H), 8.12 (s,1H), 8.09 (dd, J = 4.9 Hz), 7.79 (d, J = 1.6 Hz, 1H), 6.83 (d, J = 2.6 Hz, 1H), 6.57 (d, J = 1.6 Hz, 1H), 4.012 (s, 3H) ppm.

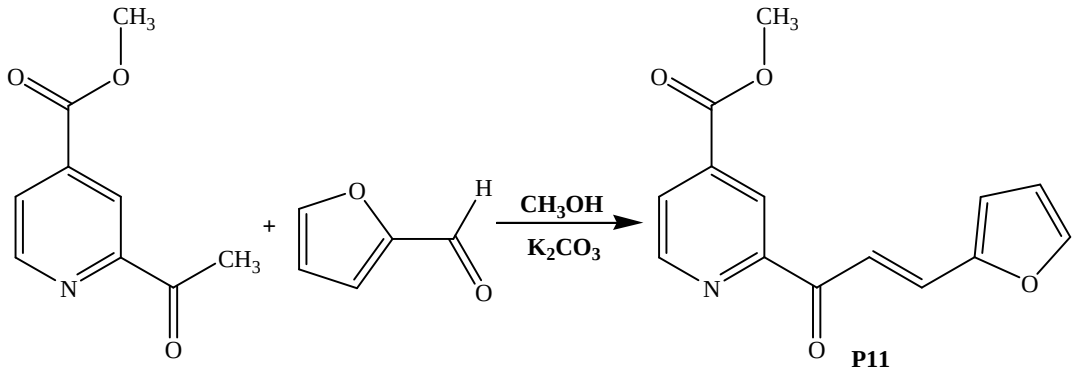

Figure 9. The scheme of enone **P11**.

2.5. Ligand L1

P1 (0.2138 g, 1.1944 mmol) was mixed with 5-hydroxymethylfurfural (0.0756 g, 0.5994 mmol) in MeOH (8 mL), 15% KOH (7.2 mL) and conc. NH_4OH (0.8 mL), as shown in Figure 10. The reaction mixture was left at room temperature to precipitate, and then the mixture was filtered and washed with 1:1 MeOH/H_2O. The mass of the collected product was 0.26 g corresponding to a 93% yield. ^{1}H-NMR (300 MHz, DMSO-d_6): δ 8.98 (d, J = 4.0 Hz, 2H), 8.67 (s, 2H), 7.98 (d, J = 4.0 Hz, 2H), 7.56 (d, J = 3.1 Hz, 2H), 6.58 (d, J = 3.1 Hz, 2H), 4.53 (s, 2H) ppm.

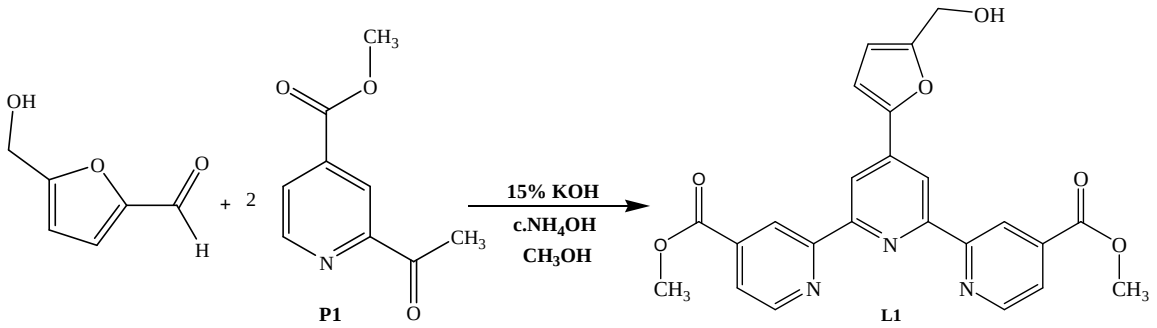

Figure 10. The scheme of ligand **L1**.

2.6. Ligand L4

Compound **P8** (0.0757 g, 0.2971 mmol) and pyridinium salt **P6** (0.1141 g, 0.2971 mmol) were mixed with NH_4OAc (0.6699 g, 8.6919 mmol) and K_2CO_3 (0.4975 g, 3.5997 mmol) in CH_3OH (10 mL), as explained in Figure 11. The reaction mixture was allowed to react for one day at room temperature, and then it was heated under reflux for 3 hours with stirring. It was left for 3 days at room temperature to precipitate, and the desired product was collected by filtration. The overall yield of the product was 0.1207 g (99%). ^{1}H-NMR (300 MHz, $CDCl_3$): δ 9.32 (s, 1H), 8.89 (d, J = 4.8 Hz,1H), 8.78 (s, 1H), 8.74 (s, 1H), 8.70 (d, J = 1.8 Hz, 1H), 8.55 (d, J = 7.0 Hz, 1H), 8.486 (d, J = 8.7 Hz, 2H), 8.11 (d, J = 1.7 Hz, 2H), 7.88 (dd, J = 1.5 Hz, 1H), 7.54 (d, J = 1.6 Hz, 1H), 7.43 (dd, J = 5.3, 6.6 Hz), 4.12 (s, 3H) ppm.

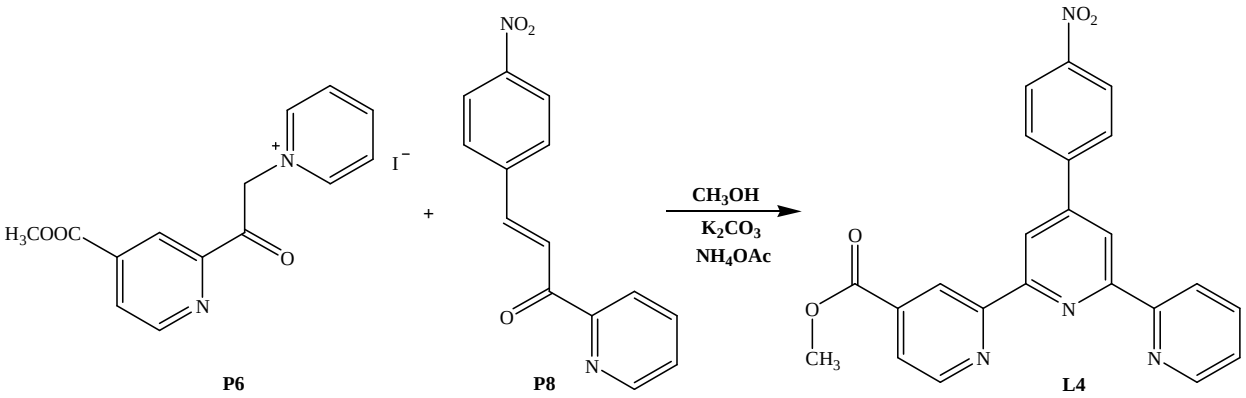

Figure 11. The synthesis of ligand **L4**.

2.7. Ligand L5

A mixture of the compound **P11** (0.1019 g, 0.3968 mmol) and the pyridinium salt **P7** (0.1293 g, 0.3968 mmol) was dissolved in CH_3OH (10 mL) with an excess of NH_4OAc (1.4 g), as is illustrated in Figure 12. The mixture was allowed to react for one day at room temperature and then heated to reflux for 3 hours with stirring. After that, the reaction mixture was left at room temperature for 3 days to precipitate, and then the precipitate was collected by filtration. The mass of the collected product was 0.0259 g corresponding to an 18% yield. ^{1}H-NMR (300 MHz, $CDCl_3$): δ 9.21 (s, 1H), 8.98 (d, J = 4.9 Hz, 1H), 8.87 (s, 1H), 8.86 (s, 1H), 8.85 (d, J = 2.7 Hz, 1H), 8.77 (d, J = 8.1 Hz, 1H), 7.98 (d, J = 1.7 Hz, 1H), 7.87 (dd, J = 2.0, 1.4 Hz, 1H), 7.66 (d, J = 7.6 Hz, 1H), 7.45 (dd, J = 5.0, 7.5 Hz, 1H), 7.23 (d, J = 3.3 Hz, 1H), 6.64 (dd, J = 1.4, 1.8 Hz, 1H), 4.12 (s, 3H) ppm.

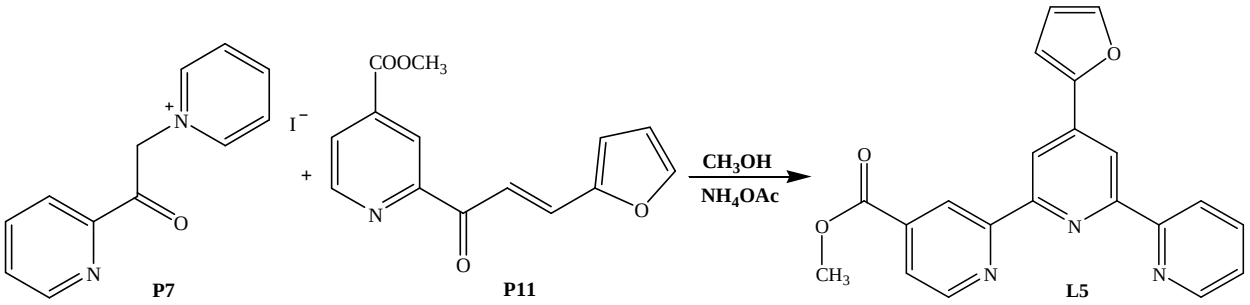

Figure 12. The synthesis of ligand **L5**.

2.8. Homoleptic Ru Complex (C1)

As shown in Figure 13, **L4** (0.0824 g, 0.1934 mmol) was mixed with $RuCl_3 \cdot 3H_2O$ (0.0261 g, 0.0998 mmol) and $AgBF_4$ (0.0584 g, 0.2999 mmol) in a 100 mL round bottom flask containing 10 mL DMF. The reaction mixture was heated at reflux overnight with stirring. The mixture was filtered free of AgCl by using Celite filter aid and rinsed with CH_3CN, and then it was evaporated by means of a rotary evaporator to remove of DMF as much as possible. After evaporating, it was dissolved in CH_3CN, and then it was slowly added to saturated aqueous solution of ammonium hexafluorophosphate (NH_4PF_6) (2 equivalents or more) to precipitate the product as a PF_6 salt. The precipitate was collected by vacuum filtration then washed with DCM to remove organic materials and with water to remove NH_4PF_6. The mass of the product obtained was 0.043 g, which corresponds to a 35% yield, and the product had a dark red color. ^{1}H-NMR (300 MHz, CD_3CN): δ 9.36 (s, 2H), 9.13 (d, J = 9.4 Hz, 2H), 8.77 (d, J = 9.3 Hz, 2H), 8.62 (d, J = 8.7 Hz, 2H), 8.45 (d, J = 1.3 Hz, 2H), 8.38 (d, J = 1.8 Hz, 2H), 8.10 (dd, J = 8.6, 7.4 Hz, 2H), 7.65 (s, 2H), 7.64 (s, 2H), 7.49 (d, J = 5.6 Hz, 2H), 7.34 (dd, J = 5.5, 6.6 Hz, 2H), 3.98 (s, 6H) ppm. ^{13}C-NMR (CD_3CN, 600 MHz), δ (ppm): 53.8, 123.5, 123.6, 123.8, 124.6, 124.9, 125.6, 125.9, 127.3, 127.6, 128.8, 130.2, 139.6, 139.9, 140.3, 143.7, 143.8, 147.4, 147.5, 150.1, 153.6, 154.5, 154.6, 156.2, 156.3, 156.7, 158.7, 160.0, 160.1, 164.6, 164.7. Mass spectrometry (ESI),

m/z: 1070.0 $[M\text{-}PF_6]^+$; 462.5 $[M\text{-}2PF_6]^{2+}$. UV-vis (CH_3CN): λ_{max} = 501 nm. FT-IR (ATR): 1734, 1599, 1522, 1344, 841 cm^{-1}.

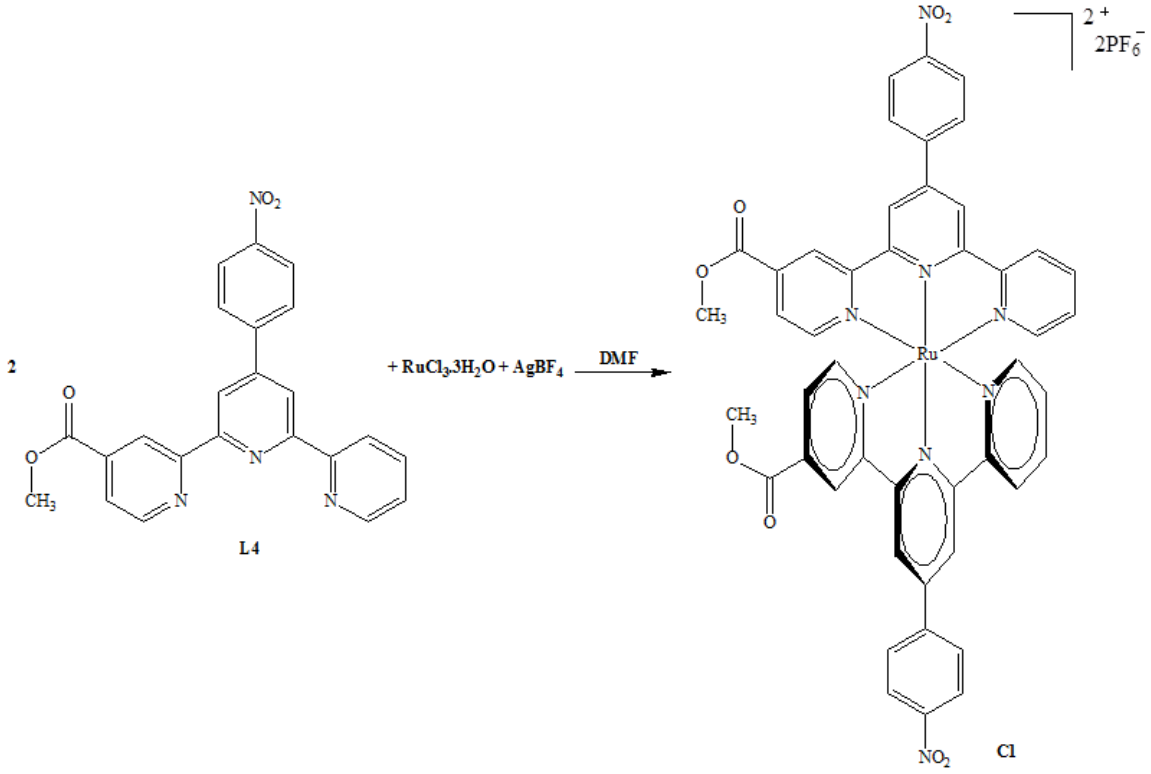

Figure 13. The synthesis of complex **C1**.

2.9. Homoleptic Fe Complex (C2)

A solution of ligand **L4** (0.2 mmol, 0.0824 g) in DMF was prepared and added to a solution of $Fe(NH_4)_2(SO_4)_2.6H_2O$ (0.1 mmol, 0.0392 g) dissolved in H_2O and DMF, and the synthesis of this complex is illustrated in Figure 14. The colour of the reaction mixture turned to a very dark purple colour. Then, the reaction mixture was added slowly to saturated aqueous solution of NH_4PF_6 (0.25 mmol, 0.0407 g). The product precipitated out of the reaction mixture, and it was collected by vacuum filtration, rinsed with $CHCl_3$ to get rid of DMF. Then, it was dissolved through the filter with acetonitrile. After evaporation, the product had a dark purple

color with a mass of 0.1031 g which corresponds to a 60% yield. ^{1}H-NMR (300 MHz, CD_3CN): δ 9.49 (d, J = 3.78 Hz, 2H), 9.36 (d, J = 2.1 Hz, 2H), 9.23 (d, J = 1.5 Hz, 2H), 8.75 (s, 2H), 8.74 (s, 2H), 8.62 (d, J = 2.9 Hz, 2H), 8.48 (s, 2H), 8.14 (dd, J = 3.8, 2.3 Hz, 2H), 7.55 (d, J = 2.1 Hz, 2H), 7.41 (d, J = 3.9 Hz, 2H), 7.19 (dd, J = 2.4, 1.3 Hz, 2H), 3.98 (s, 6H) ppm. ^{13}C-NMR (CD_3CN, 600 MHz), δ (ppm): 54.0, 123.4, 123.8, 125.3, 125.7, 126.8, 128.8, 130.3, 140.3, 140.9, 143.6, 149.6, 150.3, 154.1, 155.5, 158.4, 160.1, 161.1, 161.5, 164.7. Mass spectrometry (ESI), *m/z*: 1025.0 $[M\text{-}PF_6]^+$. UV-vis (CH_3CN): λ_{max} = 583 nm. FT-IR (ATR): 1734, 1668, 1599, 1522, 1344, 841 cm^{-1}.

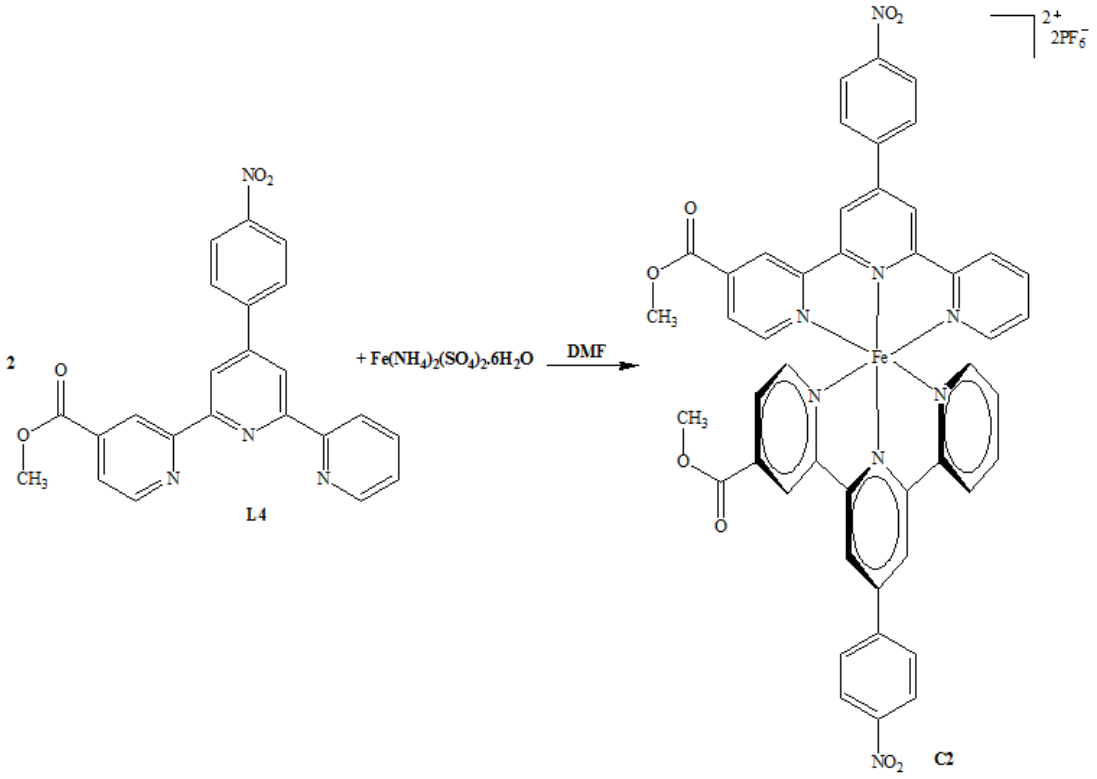

Figure 14. The synthesis of complex **C2**.

2.10. Homoleptic Fe Complex (C4)

Following the same procedure as **C2**, **L5** (0.2 mmol, 0.0714 g) and $Fe(NH_4)_2(SO_4)_2.6H_2O$ (0.1 mmol, 0.0392 g) were transformed to complex **C4** and a 99% yield (0.1540 g). In addition, this synthesis is illustrated in Figure 15. ^{1}H-NMR (300 MHz, CD_3CN): δ 9.49 (d, J = 2.7 Hz, 2H), 9.37 (d, J = 5.4 Hz, 2H), 9.23 (d, J = 4.4 Hz, 2H), 8.65 (s, 2H), 8.64 (s, 2H), 8.10 (s, 2H), 7.96 (dd, J = 8.1, 7.7 Hz, 2H), 7.68 (d, J = 3.5 Hz, 2H), 7.45 (d, J = 5.5 Hz, 2H), 7.35 (d, J = 4.5 Hz, 2H), 7.19 (dd, J = 7.4, 5.9 Hz, 2H), 6.99 (dd, J = 1.7, 1.6 Hz, 2H), 3.98 (s, 6H) ppm. ^{13}C-NMR (CD_3CN, 600 MHz), δ (ppm): 53.8, 114.2, 114.6, 118.6, 119.3, 123.5, 125.6, 126.6, 128.6, 140.1, 140.6, 140.7, 147.5, 151.3, 154.1, 155.5, 158.5, 160.2, 160.7, 161.2, 163.4, 164.7. Mass spectrometry (ESI), *m/z*: 915.0 $[M\text{-}PF_6]^+$. UV-vis (CH_3CN): λ_{max} = 588 nm. FT-IR (ATR): 1726, 1619, 839 cm^{-1}.

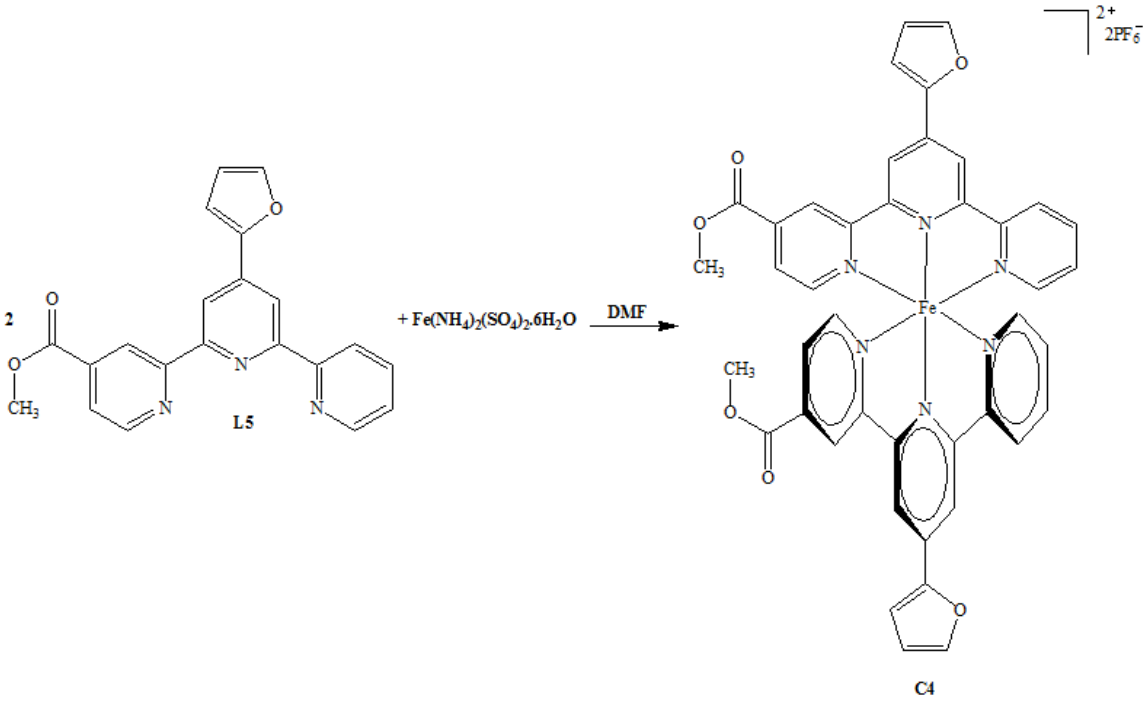

Figure 15. The synthesis of complex **C4**.

3. Results & Discussion

A large number of experiments have been carried out in pursuit of suitable ligands for our new classes of solar cell dyes.

3.1. Compound P1 (Minisci Compound/Methyl 2-Acetylisonicotinate)

The Minisci reaction places a carbonyl group on a pyridine or other nitrogenous aromatic ring. It is a transition metal-mediated radical reaction utilizing t-BuOOH as radical source and carbonyl precursors such as pyruvic acid, an aldehyde or a trioxane. Following a published procedure,[83] methyl isonicotinate was acetylated at the 2-position using excess paraldehyde (acetaldehyde trimer), excess TFA, excess t-BuOOH and catalytic $Fe_2(SO_4)_3$ at reflux for 6 hours. The synthesis of this compound **P1** is illustrated in Figure 16. The product was a very dark oil that was highly contaminated and which could not be crystallized. Chromatography revealed that the principal impurity was the 2,5-diacetylated product from evident over-reaction. A second impurity was probably the 2,6 isomer, according to NMR. While we found that we could employ this crude product in the one-pot terpyridine synthesis (see later), we could not successfully isolate either an enone or a pyridinium derivative required for the Kröhnke reaction (see below).

We reason that the products of overreaction, the 2,5 and 2,6 isomers, resulted from residual reactivity of the initial Minisci product towards the radical. The TFA in this reaction serves to protonate the pyridine nitrogen, activate the ring toward attack and direct the incoming acetyl radical to the 2-position. The product being less basic, a second acetylation is then less likely, but use of excess TFA as in the original procedure seems to promote over-reaction. In order to reduce this, we took advantage of the fact that the **P1** is less basic than the starting methyl

isonicotinate, and therefore we reasoned that we should decrease the amount of TFA present in order to reduce the propensity for the product to be protonated and then to react. This reaction has been performed many times in order to obtain product with a high level of purity, by variation of the reaction time and the quantity of TFA employed. Thus, the reaction was allowed to proceed for one-and-a-half, two, three, four and five hours. By NMR, it was determined that the purity increased with decreasing reaction time. The colour of the product also decreased, but so did the yield. After one-and-a-half hours, a significant amount of unreacted methyl isonicotinate was also present. With a two-hour reaction time, the amount of TFA was varied from > 6 equiv. to 1 equiv. to 0 equiv. The best result was obtained with one equiv. of TFA. On the other hand, the complete absence of TFA disfavoured the reaction and much starting material remained.

Having optimized the conditions (93% yield) in this manner, this reaction remained unfortunately fickle because it is a liable to gives a different yield each time even though the same conditions are used. The ^{1}H-NMR spectrum of one fairly pure product mixture was obtained and is shown in Figure 17, and it shows all the requisite hydrogen signals. However, it also shows a small amount of some additional products. As mentioned before, one of those additional products is the product of overreaction.

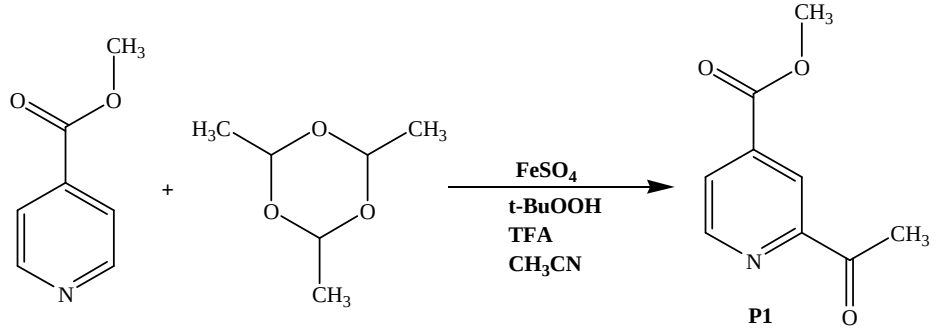

Figure 16. The synthesis of compound **P1**.

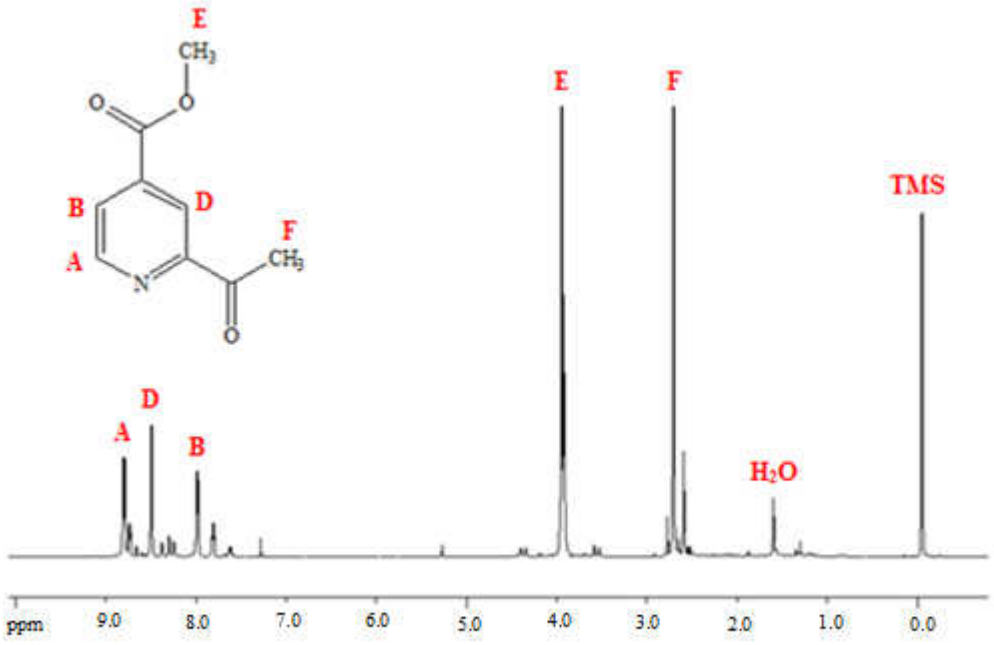

Figure 17. The ^{1}H-NMR spectrum of compound **P1** in $CDCl_3$.

3.2. Terpyridine L1

This ligand is designed to be a tridentate ligand that has three anchoring groups consisting of two carboxylic acid groups and one 2-furylmethanol group. As shown in Figure 18, Minisci product **P1** was mixed with 0.5 equiv. of 5-hydroxymethylfurfural, KOH and NH_4OH in the standard procedure that we have used many times to make symmetrical terpyridines.[86] The Product precipitated from the reaction and, filtration, necessitated no purification. The yield was 90%, and the ^{1}H-NMR spectrum of the potassium salt is given below in Figure 19. It clearly supports the structure assignment, with the furan protons giving a pair of weakly coupled signals at half the integration value of the other signals. Unfortunately, we have not had the time to return to this ligand to incorporate it into a complex.

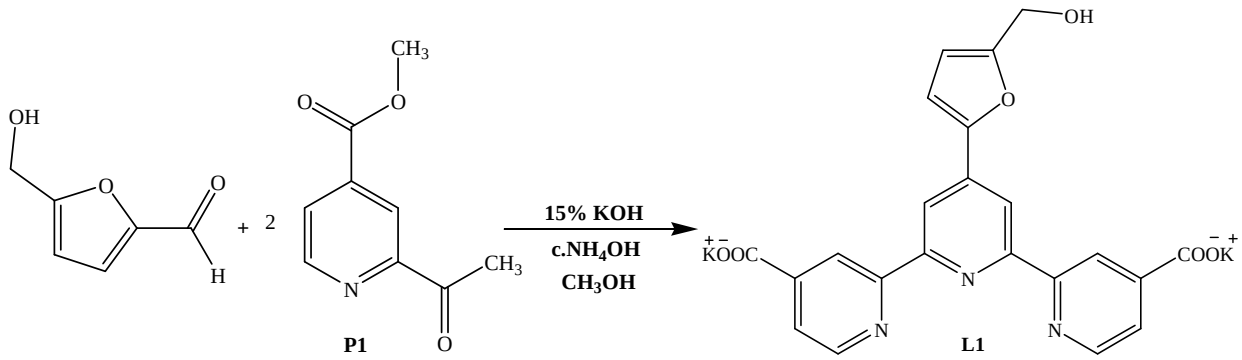

Figure 18. The synthesis of terpyridine **L1.**

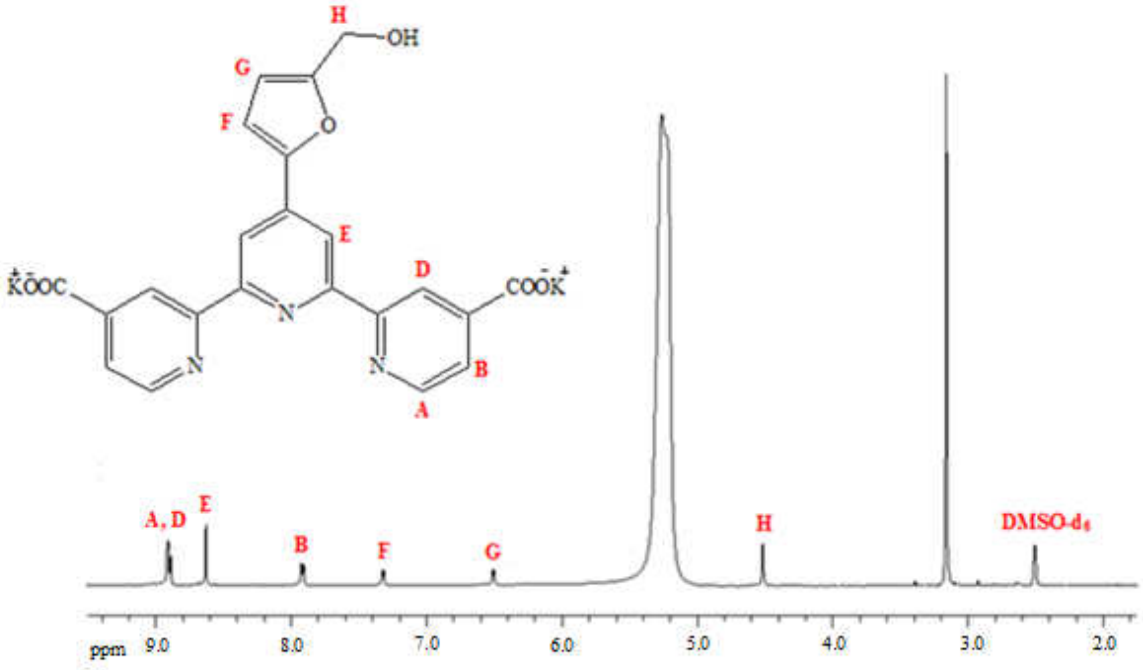

Figure 19. The ^{1}H-NMR spectrum of terpyridine **L1** in DMSO-d_6.

After synthesizing symmetrical **L1** successfully, we turned to use the Kröhnke pyridine synthesis to prepare the unsymmetrical varieties of terpyridines.[87]

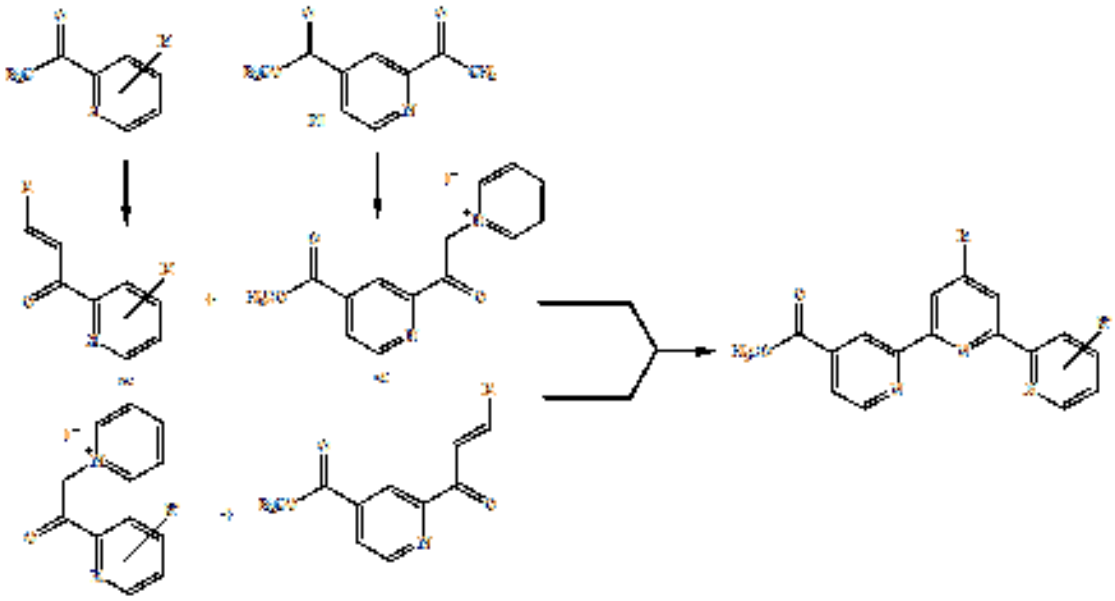

Figure 20. The Kröhnke pyridine synthesis.

The Kröhnke reaction requires a pyridinium salt and an enone in combination with a source of ammonia that typically is ammonium acetate in acetic acid or methanol.[87]

To prepare our desined ligands, two approaches were explored (Figure 20) in which the carboxylated **P1** contributes the nucleophilic component, in combination with an enone carrying a phenyl or pyridine ring, or the electrophilic component in combination with a pyridinium salt delivering the third ring. Both enones and pyridinium salts are to be prepared from the same acetylated reactants. Several of the intermediates required have already been reported in the literature, but enones derived from **P1** have not. Further, we were unable to reproduce the preparation of the known pyridinium salt from **P1**, so we needed to develop a new preparation.

3.3. Enone P2

The production of this enone was very fast; it precipitated immediately at room temperature from a mixture of N,N-dimethyl 4-aminobenzaldehyde and 2-acetylpyridine in aqueous methanol containing KOH (Figure 21). The overall yield was very high (93%), and the product had a distinctive bright orange colour. The ^{1}H-NMR spectrum a good matched with the one reported in the literature.[88]

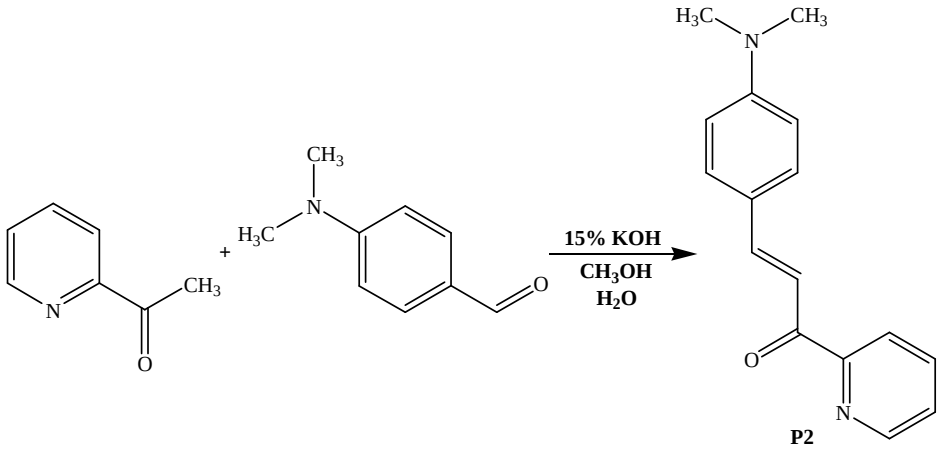

Figure 21. The synthesis of enone **P2**.

3.4. Enone P5

A similar reaction with 4-methoxyacetophenone and p-tolualdehyde was also successful, and the synthesis of this enone **P5** is illustrated in Figure 22. The overall yield was very good (83%), and the ^{1}H-NMR spectrum matched that reported in the literature.[89]

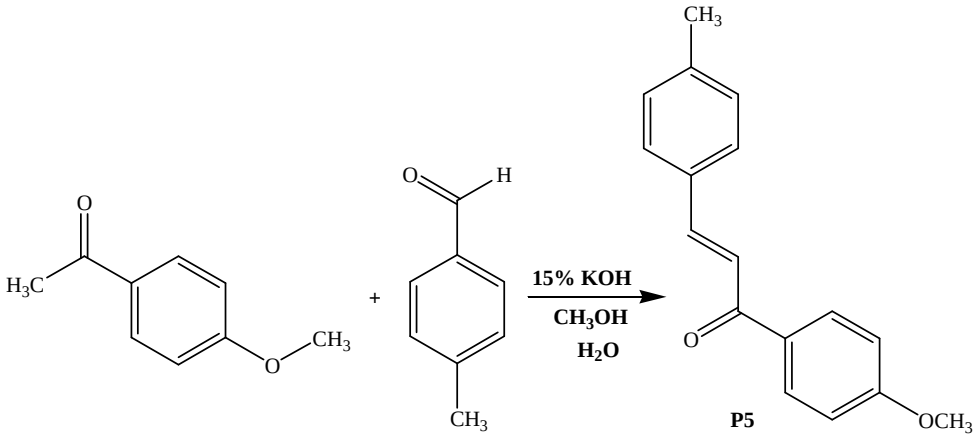

Figure 22. The synthesis of enone **P5**.

3.5. Enone P8

The aim here was to prepare an enone that would more reactive than enone **P2**. The production of this compound was very fast; it precipitated immediately at room temperature from a mixture of 4-nitrobenzaldehyde and 2-acetylpyridine in aqueous methanol containing KOH. Figure 23 illustrates the synthesis of this enone **P8**. The overall yield was very high (97%), and the ^{1}H-NMR spectrum matched that reported in the literature.[90]

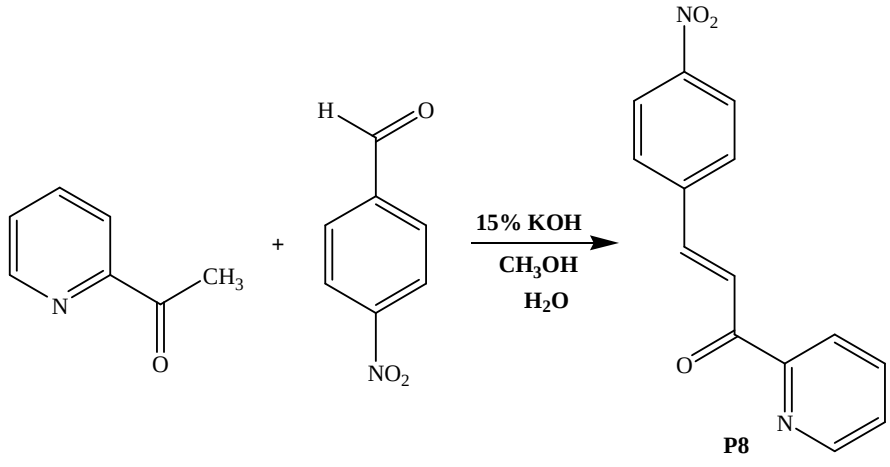

Figure 23. The synthesis of enone **P8**.

3.6. Enone P10

We made many attempts to produce this enone, in both aqueous conditions and non-aqueous conditions. We wished to ideally produce this compound in non-aqueous conditions so as to avoid hydrolysis of the ester group of the Minisci product **P1** when converting it to **P11**. We therefore used the synthesis of non-carboxylated **P10** as an inexpensive model reaction with which to develop non- aqueous conditions.

The non-aqueous condition was a mixture of 2-acetylpyridine and furfural in methanol and potassium carbonate, at reflux for two hours or at room temperature. None of these attempts worked successfully. In comparison, the aqueous condition worked very well; it precipitated immediately at room temperature from a mixture of 2-acetylpyridine and furfural in aqueous methanol containing KOH (Figure 24). The overall yield from two crops was very good (90%), and the ^{1}H-NMR spectrum matched that in the literature.[91]

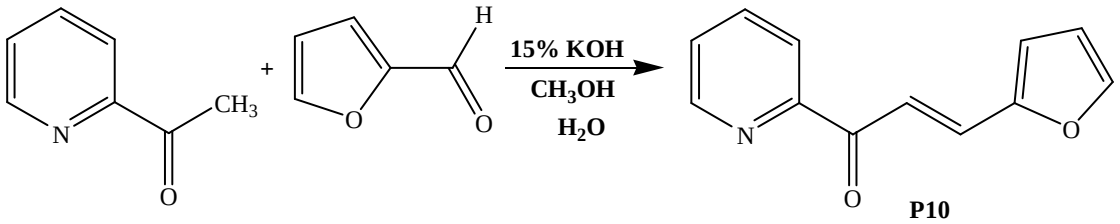

Figure 24. The synthesis of enone **P10**.

3.7. Enone P11

Despite the failure to make **P10** in non-aqueous environment, we carried on the search for non-aqueous conditions suitable to the preparation of **P11**. A mixture of furfural and Minisci product **P1** was dissolved in dry CH_3OH and treated with excess K_2CO_3, and the reaction

mixture was set to reflux for two hours. This attempt resulted in hydrolysis (absence of an ester peak at 4 ppm in the NMR spectrum and poor solubility). Therefore, this reaction was performed with Diisopropylamine instead of potassium carbonate in order to avoid the hydrolysis. Unfortunately, there were some starting material signals in the ^{1}H-NMR spectrum, indicating a poor conversion.

The successful method of synthesizing this enone while avoiding hydrolysis was accomplished in dry CH_3OH using K_2CO_3 at room temperature, illustrated in Figure 25. The product started to precipitate after 10 minutes. Despite the temptation to allow precipitation to continue, it should be collected promptly. If allowed to stand, the precipitate redissolves eventually, and the worked-up crude product. The overall yield of the initial precipitate was not very satisfactory (34%) but the material was very pure. The ^{1}H-NMR spectrum of the enone **P11** is shown in Figure 26.

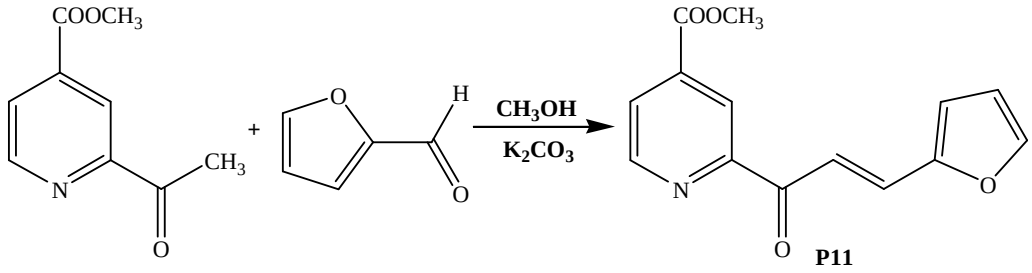

Figure 25. The synthesis of enone **P11**.

The spectrum showed all of the requisite signals, including a strongly coupled AB pair (E, F) indicative of a trans alkene moiety.

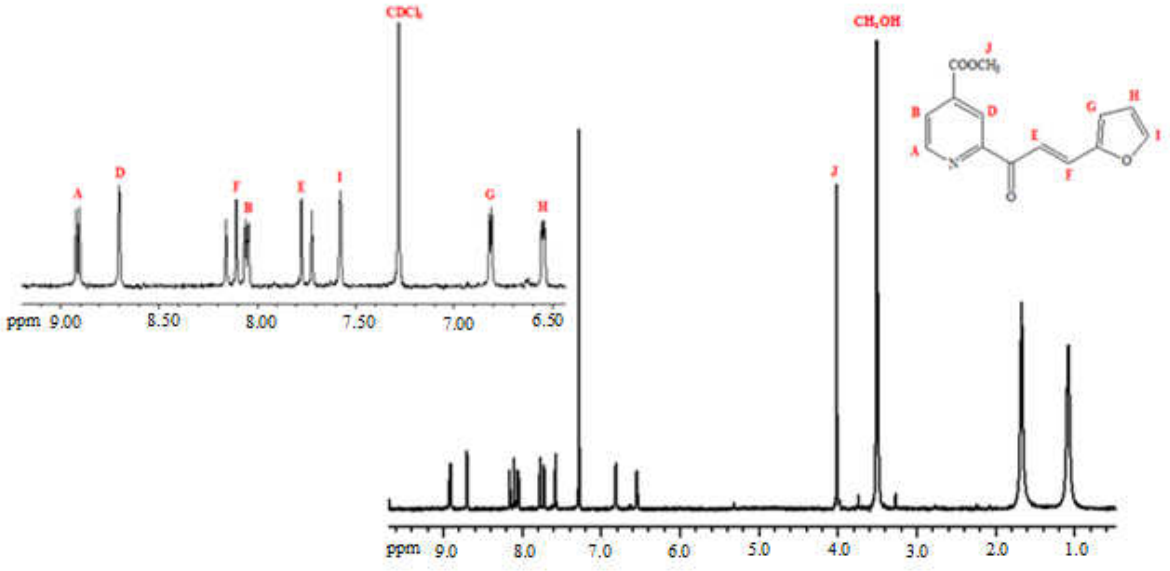

Figure 26. The ^{1}H-NMR spectrum of enone **P11** in $CDCl_3$.

3.8. Enone P3 and other unsuccessful targets

Enone **P3** is similar to **P2**, but bears a $COOCH_3$ group derived from **P1**. In accord with our design objectives, this target features an electron-donating group to render the central ring of our ligands relatively electron-rich.

To maintain the ester group, we explored a variety of non-aqueous conditions employing catalytic base ($^{i}Pr_2NH$ or NaH) or acid (pTsOH) in THF or toluene at reflux, sometimes for many days. In none of these attempts was the desired condensation product obtained, however. Similarly, reactions with some other aldehydes (furfural, pyrrole-2-carboxaldehyde, 4-methoxybenzaldehyde) also failed, with either 2-acetylpyridine or Minisci product **P1**. In some cases, product was obtained but NMR suggested the formation of 3:2 or 3:1 condensation products, as had been found to be commonplace.[83] Some reaction optimization will be required to avoid such by-products.

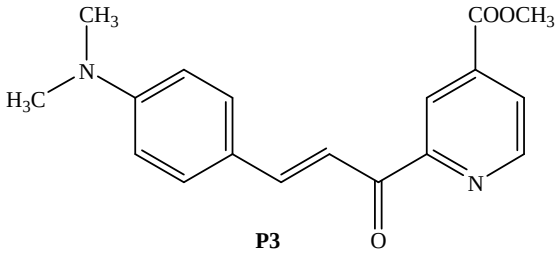

P3

3.9. Enone P4

Enone **P4** was destined to provide a dicarboxylated analogue of black dye. To synthesize this enone with the two ester groups, we employed a variety of conditions. A simple mixture of 4-carboxybenzaldehyde and **P1** was dissolved in aqueous methanol containing KOH and left at room temperature, followed by reflux for more than 9 hours.

Ester hydrolysis was, of course, expected but we intended to esterify the carboxy group in a second step in any case. However, the crude product showed consumption of the aldehyde but no sign of the desired enone. In a second attempt, a mixture of 4-carboxybenzaldehyde and **P1** in EtOH was treated with catalytic NaH. The crude product was insoluble in $CDCl_3$, unsurprisingly, but unfortunately, the only D_2O-detectable product appeared to come solely from 4-carboxybenzaldehyde but lacked the aldehyde group.

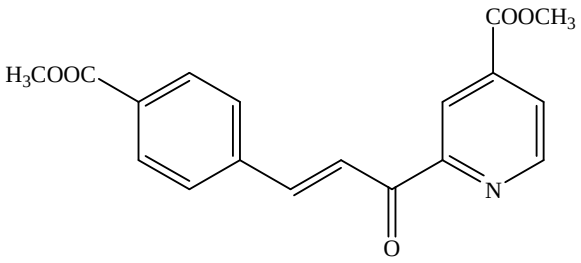

P4

3.10. Enone P9

This enone is similar to **P8**, but bears a $COOCH_3$ group derived from **P1**. A mixture of 4-nitrobenzaldehyde and 2-acetylpyridine was dissolved in CH_3OH and treated with K_2CO_3 at room temperature, and left to react for many days. The ^{1}H-NMR spectrum of the crude product showed no sign of **P9**, it showed starting products.

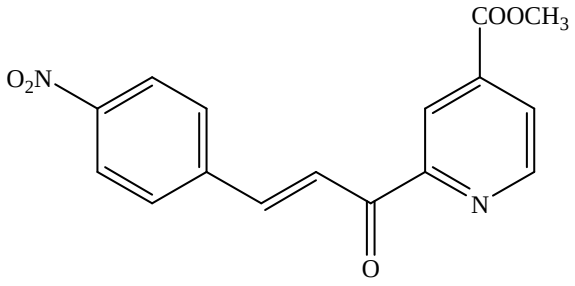

P9

3.11. Enone P12

This enone would also be destined to provide a dicarboxylated analogue of black dye. To synthesize this enone, a mixture of **P1** and glyoxylic acid was dissolved in aqueous methanol containing KOH and left at room temperature. To obtain the ^{1}H-NMR, we tried many different solvents to dissolve it. Unfortunately, these attempts did not work very well.

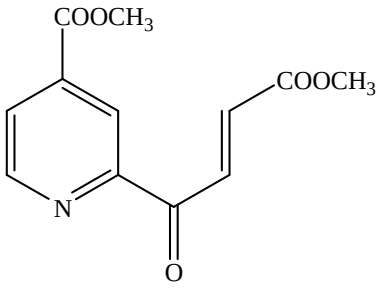

P12

We were unable to generate an enone containing a second carboxylic group which is needed for the design $\mathbf{C_A}$. However, we knew that a furan ring can be converted into a carboxylic group.[92] Thus, the furan ring stands in for a carboxylic group, and then it can be used in the synthesis of the $\mathbf{C_A}$ type complex or can stay put for a $\mathbf{C_D}$ type complex and act as an electron-donating ring.

3.12. Pyridinium Salts P6 and P7

Several attempts were made to convert the Minisci product **P1** to the known pyridinium salt **P6** by the literature procedure.[83] This procedure is modeled on the original Kröhnke work. It uses I_2 in pyridine as solvent with heating under reflux for 3 hours, with precipitation of the product. In our hands, the NMR spectrum of the precipitate corresponded to the desired salt, but it was always contaminated with pyridinium iodide (or triiodide). No such difficulty was encountered when using simple 2-acetylpyridine or acetophenone.

There was no means to purify this salt with co-precipitation, however we found a good method to produce the salt at a high level of purity, following the procedure in a second literature report.[85] According to this, the reaction mixture should be placed in an oil bath preheated at 130°C, which should then solidify after only 8 min, and continuing to heat for another minute.

However, we modified this protocol and our reaction mixture was heated under reflux for 9 min (Figure 27). Then it was allowed to cool at room temperature and left for many days for precipitation. The overall yield of this pyridinium salt was decent (55%).

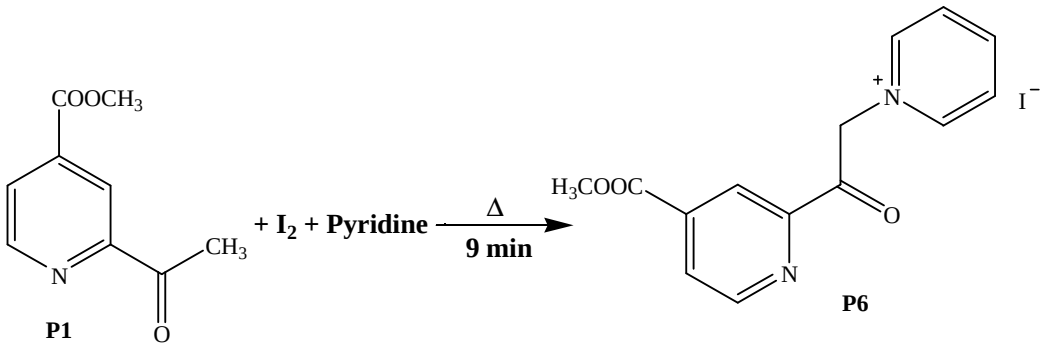

Figure 27. The synthesis of pyridinium salt **P6.**

The ^{1}H-NMR spectra for this pyridinium salt **P6** is shown in Figure 28. The spectrum is much cleaner and all of the signals expected from **P6** are present.

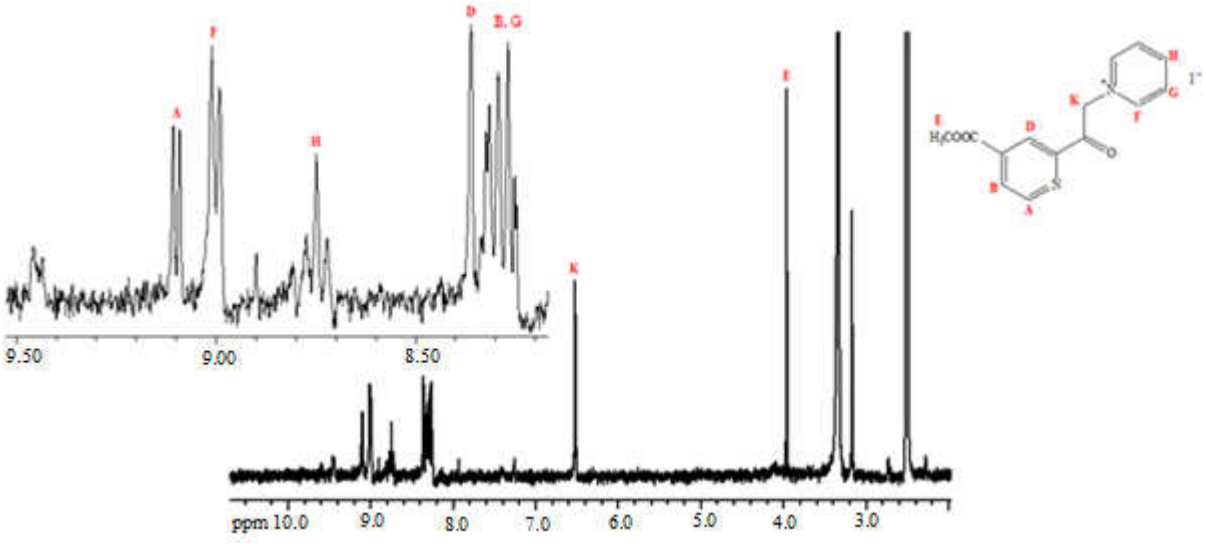

Figure 28. The ^{1}H-NMR spectra of pyridinium salt **P6** in DMSO-d_6.

Using the same modified procedure, we were able to produce pyridinium salt **P7** (Figure 29) from 2-acetylpyridine with an even higher level of purity than **P6**, and the overall yield was also very good (61%). The ^{1}H-NMR spectra for **P7** is shown in Figure 30.

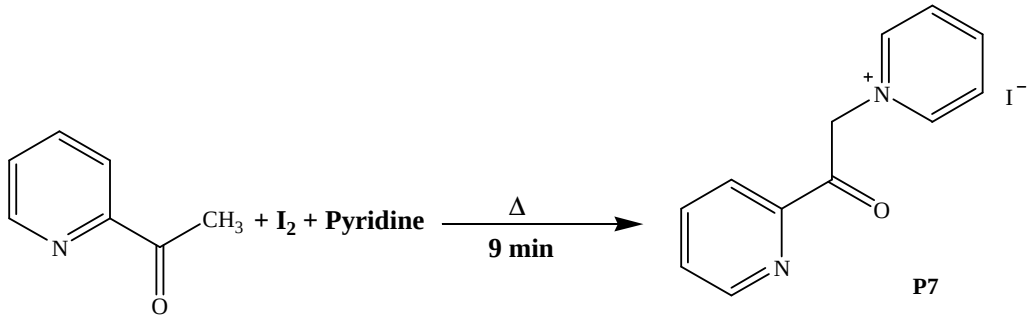

Figure 29. The synthesis of pyridinium salt **P7.**

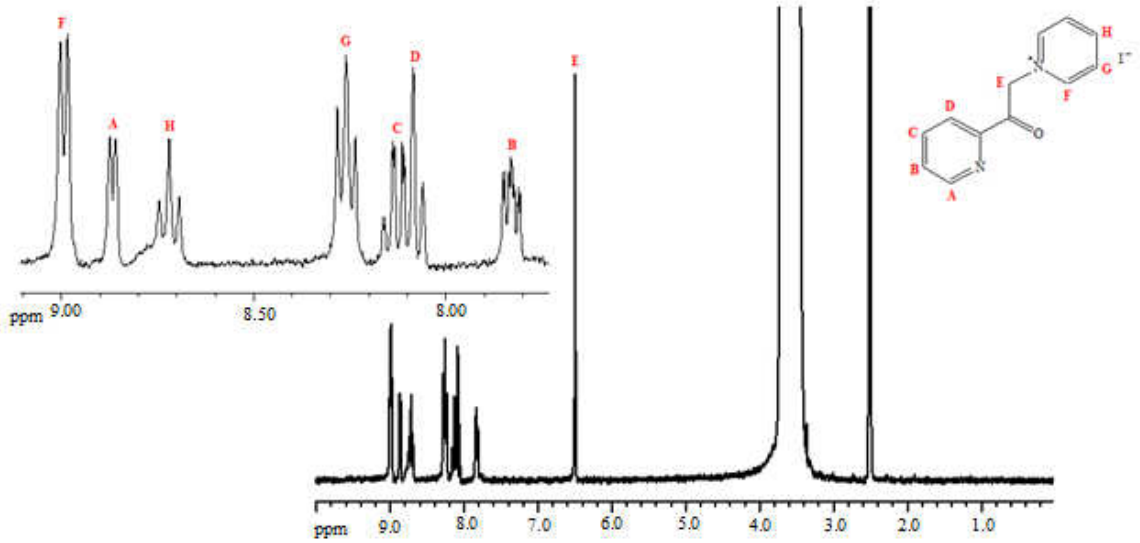

Figure 30. The ^{1}H-NMR spectra of pyridinium salt **P7** in DMSO-d_6.

3.13. Terpyridines L2 and L6

Several attempts were made to synthesize **L2** bearing an electron-donating amino group. Table 1 lists the conditions used. In one of several attempts, the Minisci product **P1** was mixed

with enone **P2** in CH_3OH containing KOH and NH_4OAc at room temperature. We also tried a reaction in THF, containing two drops of the strong base DBU at reflux for one day. A third more direct attempt used **P1** was mixed with 2-acetylpyridine and 4-dimethylaminobenzaldehyde (1:1:1) ratio in CH_3OH containing KOH and c. NH_4OH at room temperature. This was also carried out using Hanan's conditions[93] (EtOH, solid KOH, NH_4OAc) at room temperature. In the last attempt, a mixture of enone **P2** and pyridinium salt **P6** was dissolved in CH_3OH containing NH_4OAc and K_2CO_3 and left at room temperature for one day, then heated to reflux for 3 hours. Unfortunately, none of these attempts furnished the desired product. In some cases, NMR showed that there were 2 or 3 products, and none of them was the desired product.

Table 1. Reactants and conditions used in attempted Kröhnke reactions.

Reactants	**Conditions**
P1 and **P2**	CH_3OH, KOH and NH_4OAc
P1 and **P2**	THF, and DBU
P1, 2-acetylpyridine and 4-dimethylaminobenzaldehyde	CH_3OH, KOH and NH_4OAc
P1, 2-acetylpyridine and 4-dimethylaminobenzaldehyde	EtOH, solid KOH and NH_4OAc
P2 and **P6**	CH_3OH, NH_4OAc and K_2CO_3

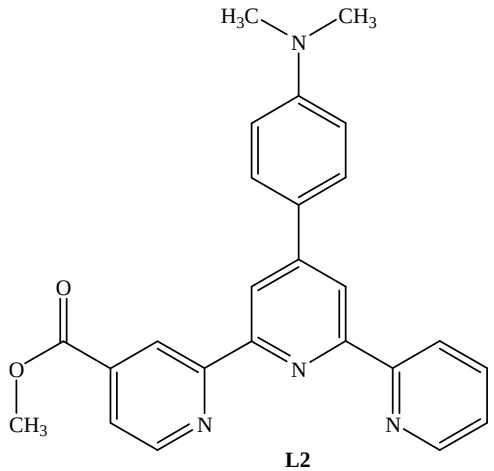

L2

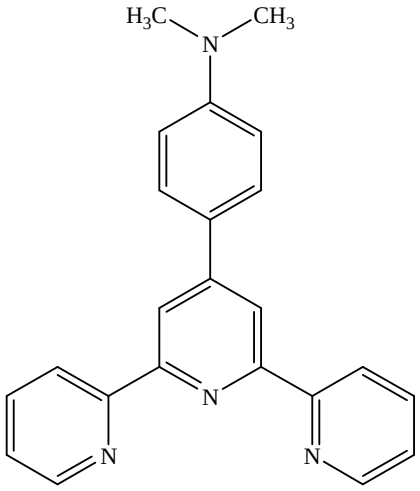

L6

Taking a step back, we decided to generate the model **L6** which lacks the carboxyl group of **L2**. This ligand is already known, and we repeated the procedure reported in the literature. [93] The overall yield was not very high (45%), and the product had a distinctive bright green colour. The ^{1}H-NMR spectra matched that reported in the literature.[93]

3.14. Terpyridine L3 and L7

To produce this ligand, we employed two different reaction conditions using the same mixture of compound **P1** and **P5**. In the first trial, the mixture was dissolved in CH_3OH and treated with 15% KOH and c. NH_4OH at room temperature. The ^{1}H-NMR spectrum showed only the presence of starting **P1**. In the second attempt, NH_4OAc and solid KOH were used in EtOH. However, the crude ^{1}H-NMR spectrum showed that this reaction produced a very complex mixture.

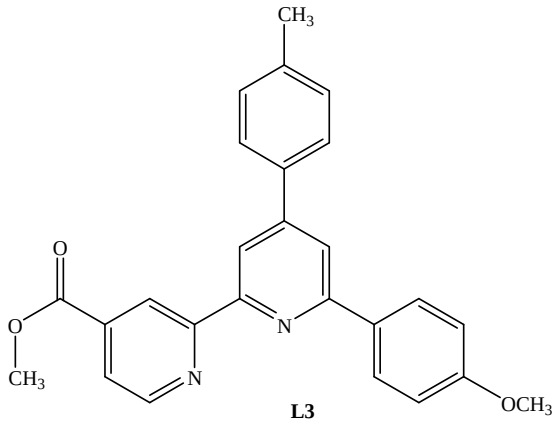

L3

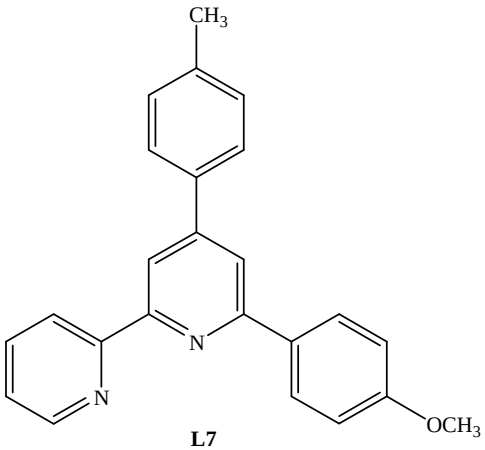

L7

We also attempt to produce the simpler **L7** which lacks the carboxyl group, and this is a known compound**.** However, we could not obtain this product by the procedure that was reported in the literature.[94]

3.15. Terpyridine L4 and L8

In the first attempt at ligand **L4**, Minisci product **P1** was mixed with 2-acetylpyridine and 4-nitrobenzaldehyde with 15% KOH and c. NH_4OH in CH_3OH at room temperature. The second trial involved a mixture of compound **P8,** pyridinium salt **P6** and NH_4OAc in CH_3OH, which was refluxed gently for two hours. Sadly, these attempts were unsuccessful.

However, after extensive optimization, we were able to establish a good method to produce the desired **L4**. A mixture of compound **P8,** pyridinium salt **P6,** NH_4OAc and K_2CO_3 in CH_3OH was allowed to react for one day at room temperature, then at reflex for 3 hours. It was then left for 3 days at room temperature to precipitate, and then the desired product was collected by filtration. The ^{1}H-NMR spectra of this ligand (Figure 32) confirms that it is the desired product, and the overall yield was very high (99%) as well.

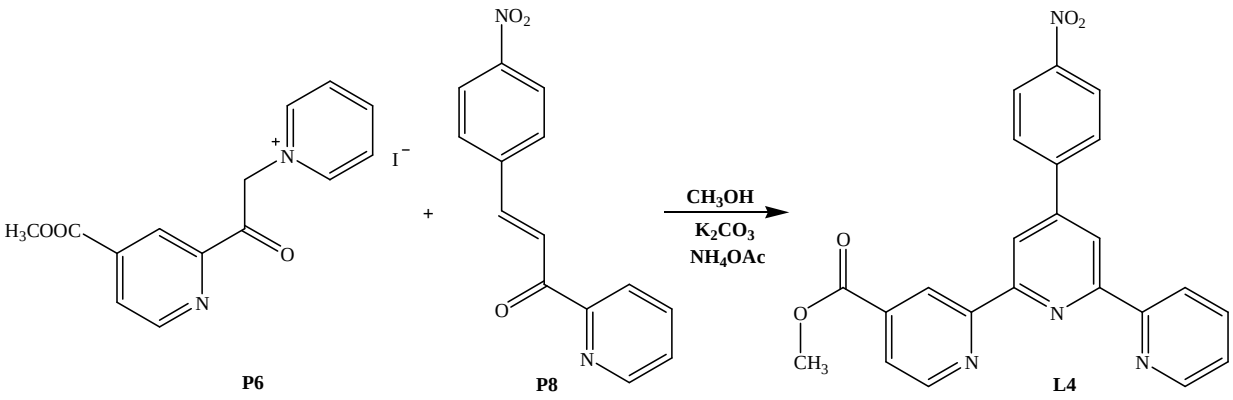

Figure 31. The synthesis of terpyridine **L4.**

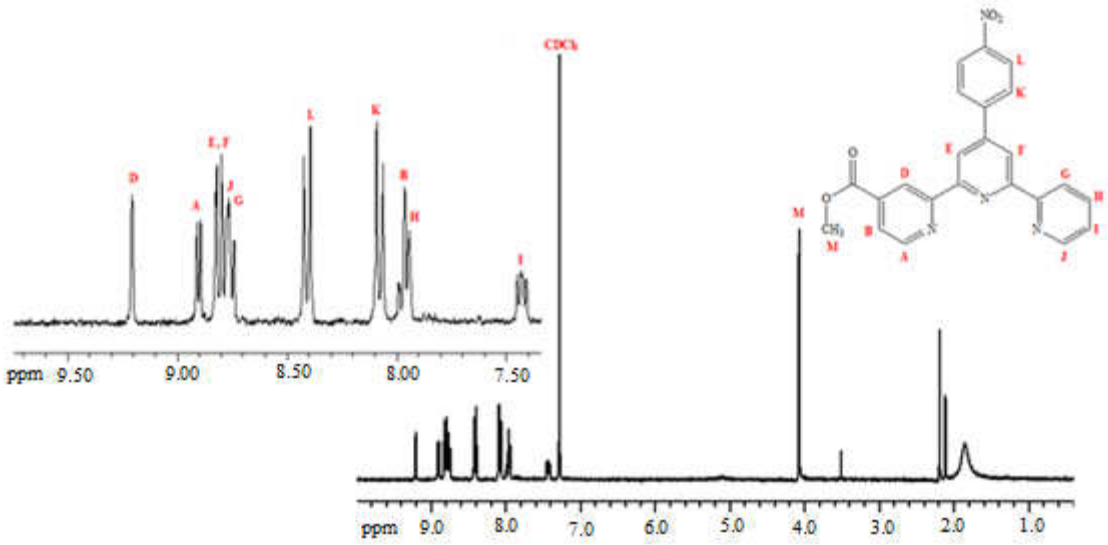

Figure 32. The ^{1}H-NMR spectra of terpyridine **L4** in $CDCl_3$**.**

The preparation of the simpler **L8** lacking the carboxyl group following the procedure reported in the literature also worked.[84]

The interest in this product lies in the fact that the nitro group of this ligand can be easily reduced to amine group using one of several different reagents in order to obtain a new ligand

with an electron-donating aniline group, since we were unable to prepare the dimethylamine analogue directly.

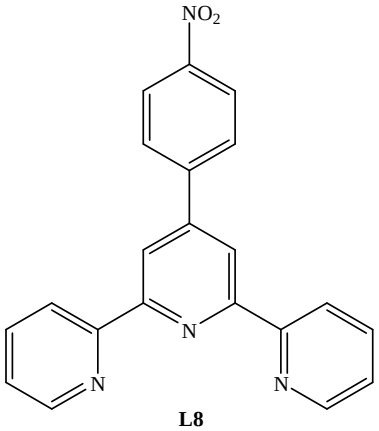

L8

3.16. Terpyridine L5 and L9

Several attempts have been performed to synthesize this ligand while maintaining the ester group. In the first attempt, intended to trap the 1,5-diketone intermediate, 2-acetylpyridine was mixed with the compound **P11** in CH_3OH containing NH_4OAc and K_2CO_3, either at room temperature or at reflux for two hours, or even for more than two hours. The crude product showed NMR signals consistent with **L5** but it was contaminated with another product containing a pyridine ring and an ester group. In the face of this part success, we tried two sets of reagents that would sacrifice the ester group (15% KOH, NH_4OH, CH_3OH or solid KOH, NH_4OH, and EtOH at room temperature or at reflux), but in all cases the only detectable product was 2-acetylpyridine. In an alternative, even more direct approach, a mixture of 2-acetylpyridine, Minisci product **P1**, and furfural (1:1:1) ratio was allowed to react with 15% KOH and NH_4OH in CH_3OH for 3 days at room temperature, followed by filtration and washing with $MeOH/H_2O$ (1:1). The rationale for this attempt was the hope that P1 would more easily form the enolate and

undergo aldol condensation with the aldehyde before the involvement of 2-acetylpyridine. Unfortunately, this strategy failed as the collected product appeared the symmetrical terpyridine derived from 2-acetylpyridine and furfural, according to NMR.

In the next attempt, the complimentary pair of Kröhnke reagents that are the enone **P11** and the pyridinium salt **P7** were dissolved in CH_3OH containing NH_4OAc, and the solution was heated under reflux for two hours. This produced a complex reaction mixture. Several other variations were also explored, such as NH_4OAc and Ac_2O (to trap moisture) in AcOH with heating for 2 hours, which resulted in an insoluble product lacking the desired ester group, or NH_4OAc and K_2CO_3 in CH_3OH at room temperature, which produced a complex mixture of products, one or more of which showed unexpected aliphatic signals. The opposite combination, using compound **P10** and pyridinium salt **P6**, also failed, again producing an undecipherable product mixture.

However, after all of these unsuccessful attempts, we finally found a suitable method to produce the desired product, illustrated in Figure 33. A mixture of compound **P11** and pyridinium salt **P7** was dissolved in CH_3OH and treated with an excess of NH_4OAc. The mixture was allowed to react for one day at room temperature and then at reflux for 3 hours. After that, the reaction mixture was left at room temperature for 3 days before filtration of the product. Though the overall yield of **L5** was not very satisfactory (18%), it was very pure. The ^{1}H-NMR spectra of terpyridine **L5** are shown in Figure 34. As mentioned earlier, the furan ring can be oxidized to a carboxylic acid.[92]

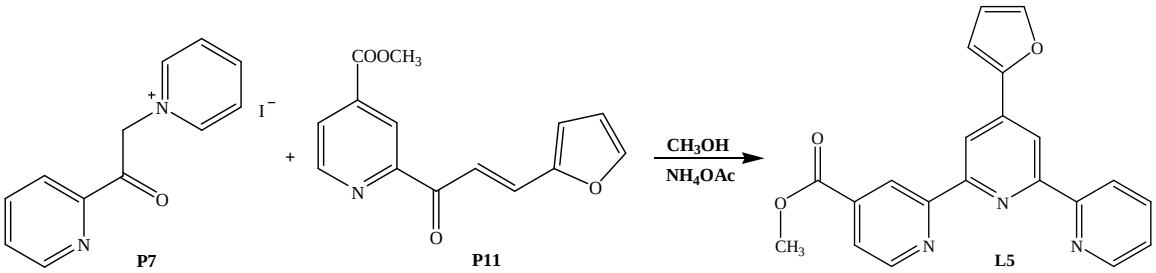

Figure 33. The synthesis of terpyridine **L5.**

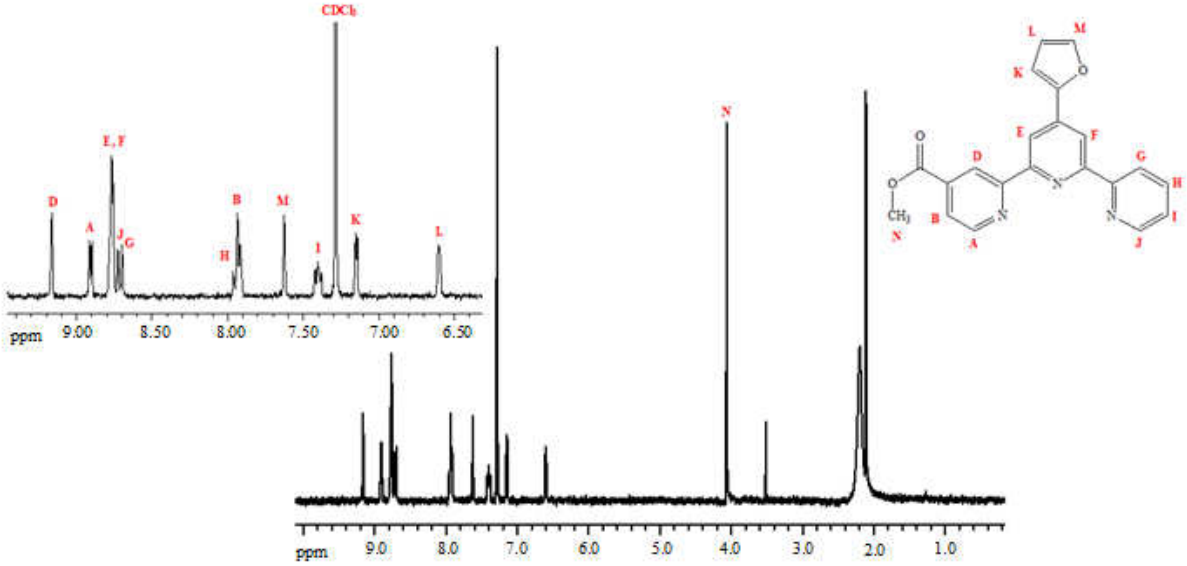

Figure 34. The ^{1}H-NMR spectra of terpyridine **L5** in $CDCl_3$**.**

We also tried to produce **L9** that lacks the carboxyl group and this is a known compound**.** However, we were unable to obtain this product by the procedure that was reported in the literature.[95]

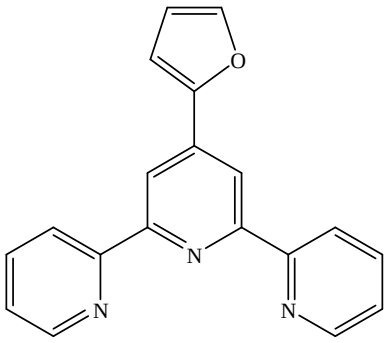

L9

In addition, we made other attempts at the ligands using enone **P10** and 2-acetylpyridine under many different conditions. These attempts varied the base catalyst ($^{i}Pr_2NH$ or K_2CO_3), the source of NH_3 (NH_4OAc, NH_4Cl or NH_4PF_6) and the solvent (THF, CH_3CN, or CH_3OH). In some cases, the reaction mixture was allowed to proceed without the NH_4OAc, NH_4Cl or NH_4PF_6 in order to prepare the 1,5 diketone intermediate. These attempts were performed at room temperature, with heating under reflux for 2 hours and sometimes for more than 2 hours. We also tried using K metal in CH_3OH or acidic conditions (CH_3COOH, NH_4OAc, Ac_2O). Sadly, all of these attempts failed.

3.17. Homoleptic Ru Complex (C1)

A mixture of **L4**, $RuCl_3 \cdot 3H_2O$ and $AgBF_4$ was heated overnight in DMF, and then the product was precipitated as a PF_6 salt. The overall yield of the product was not very high (35%). The ^{1}H-NMR spectra of this complex (**C1**) which are shown below (Figure 36) was fully consistent with the desired structure. It did not show as much asymmetry as the spectrum of **L4**.

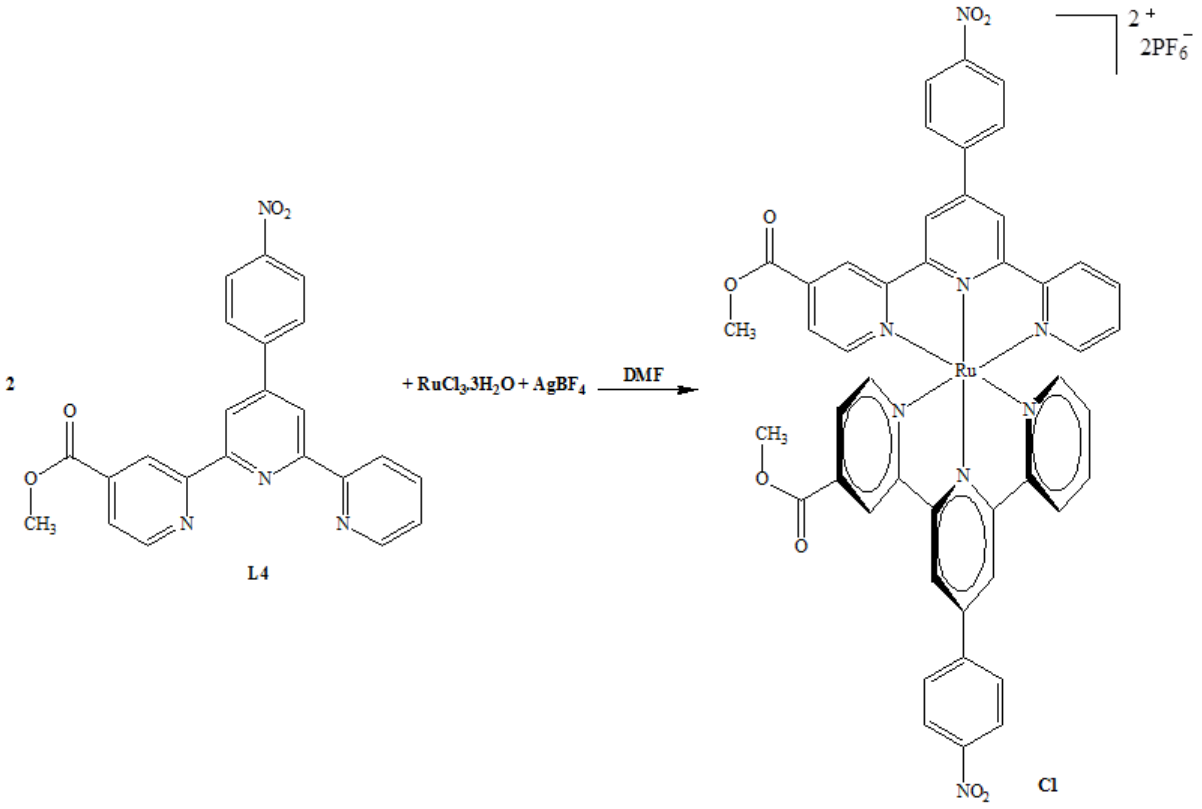

Figure 35. The synthesis of complex **C1.**

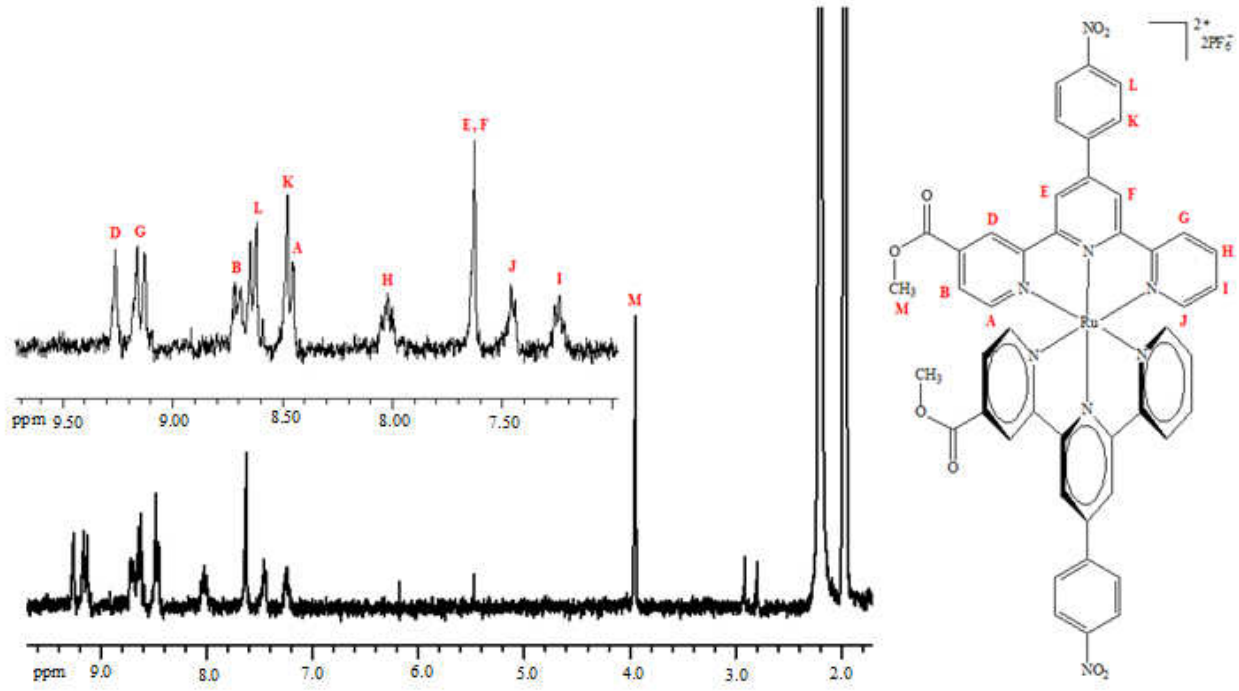

Figure 36. The ^{1}H-NMR spectra of complex **C1** in CD_3CN**.**

In addition, the ^{13}C‑NMR spectrum was also obtained (Figure 37), and it showed all the requisite carbon signals, confirming the absence of local symmetry.

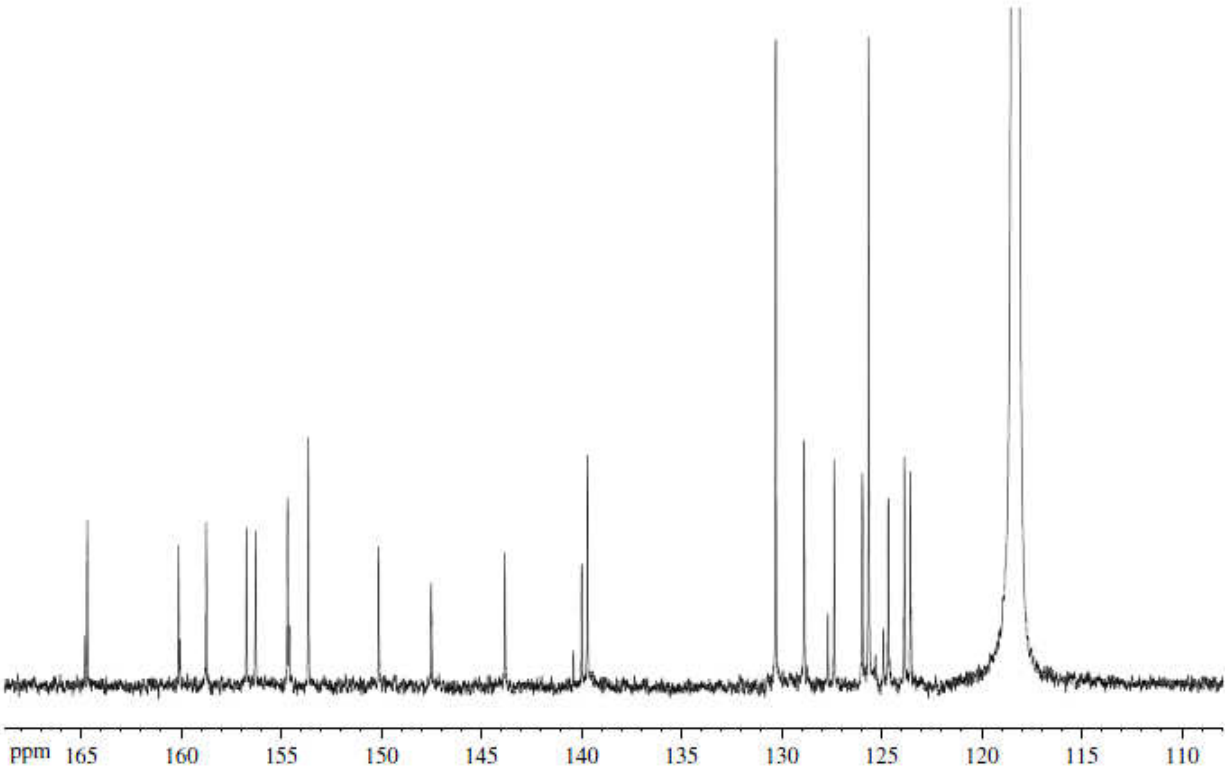

Figure 37. ^{13}C-NMR spectrum of **C1** in CD_3CN.

The IR spectrum (Figure 38) confirms the presence of PF_6, and it also shows the carbonyl and nitro stretches.

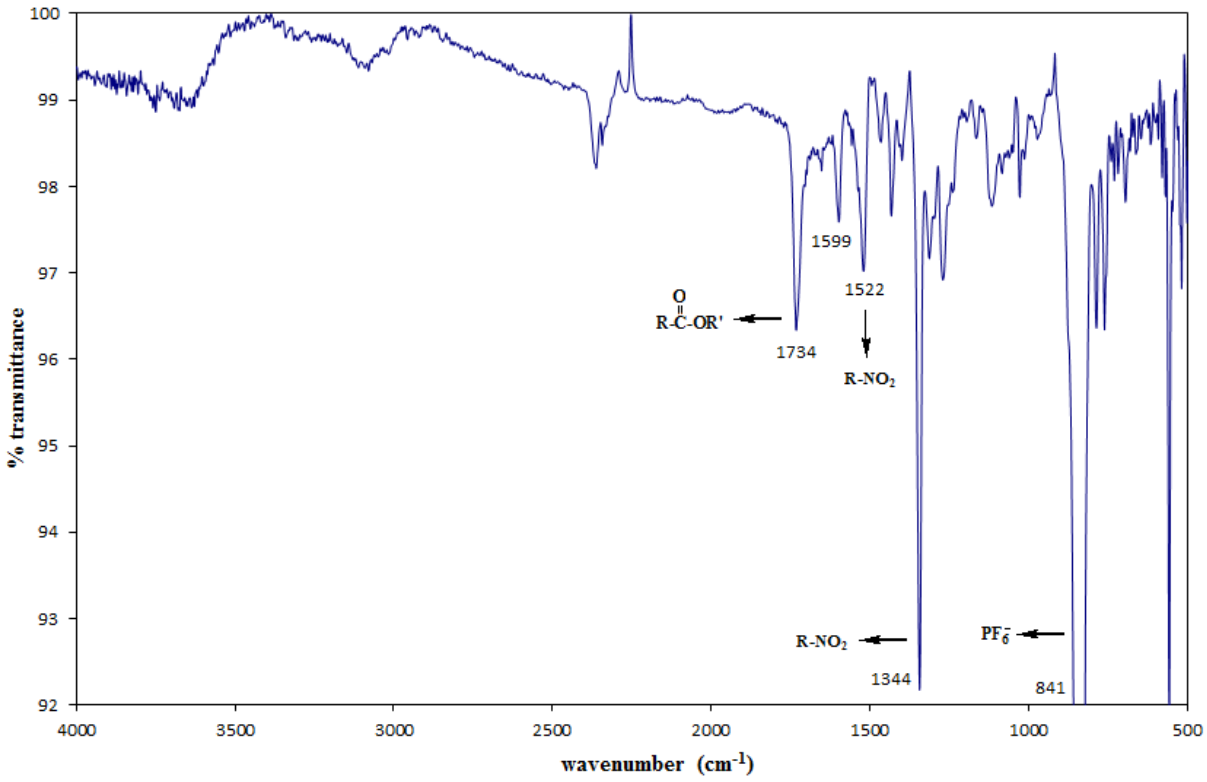

Figure 38. FT-IR spectrum for the complex **C1.**

The ESI-MS spectrum for **C1** showed two diagnostic clusters. The first cluster showed a doubly charged species corresponding to $[(\mathbf{C1})_2Ru]^{2+}$, and the experimental spectrum has the same isotopic distribution as the calculated one (Figure 39). In addition, the second cluster corresponded to $\{[(\mathbf{C1})_2Ru](PF_6)\}^{+}$, also with an isotopic distribution matching well with that expected for the proposed formula (Figure 40).

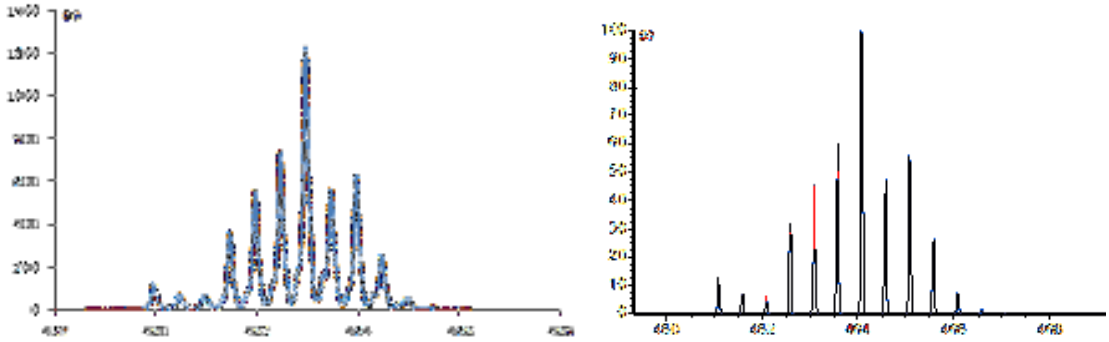

Figure 39. Mass spectrum of **C1** cluster $[(\mathbf{C1})_2Ru]^{2+}$ in CH_3CN:

at left, experimental; at right, calculated.

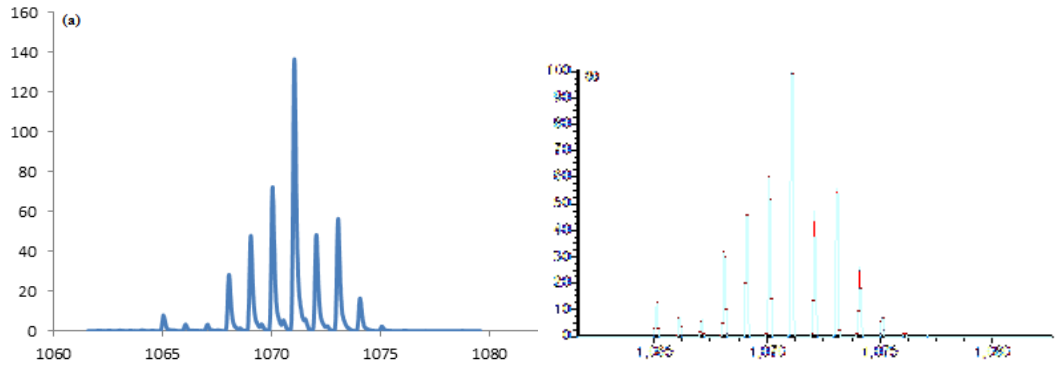

Figure 40. Mass spectrum of **C1** cluster $\{[(\mathbf{C1})_2Ru](PF_6)\}^+$ in CH_3CN:
at left, experimental; at right, calculated.

3.18. Homoleptic Fe Complex (C2)

The second design (**C2**) is of a homoleptic iron complex and a terpyridine-based ligand bearing one carboxylic acid group and a nitrobenzene group. Several attempts have been made to synthesize this complex in various solvents (MeOH, CH_3CN, acetone) but the best solvent found was DMF. The ligand **L4** solution was treated with the iron salt dissolved in H_2O and DMF. The colour of the reaction mixture changed to very dark purple colour. Then, the reaction mixture was added slowly to saturated aqueous solution of NH_4PF_6 to precipitate the product. The overall yield was good (60%). The ^{1}H-NMR spectrum is shown in Figure 42. Although showing only broad signals, was not inconsistent with the desired structure.

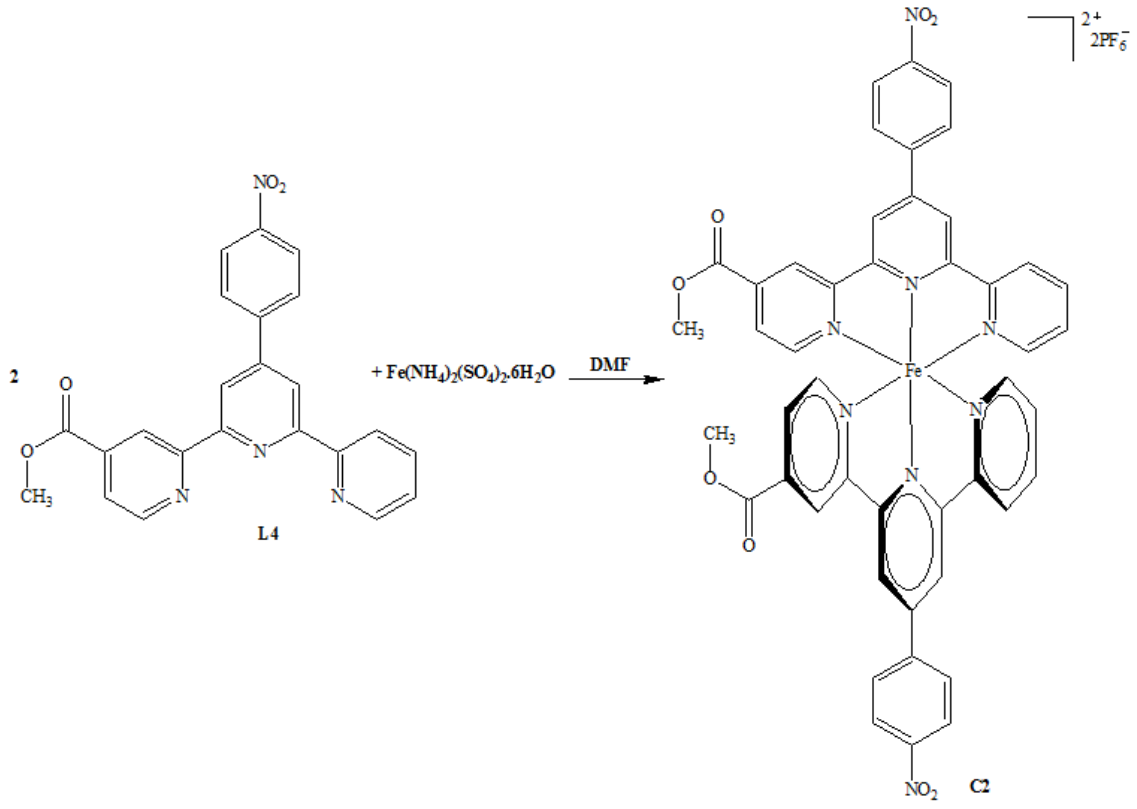

Figure 41. The synthesis of complex **C2**.

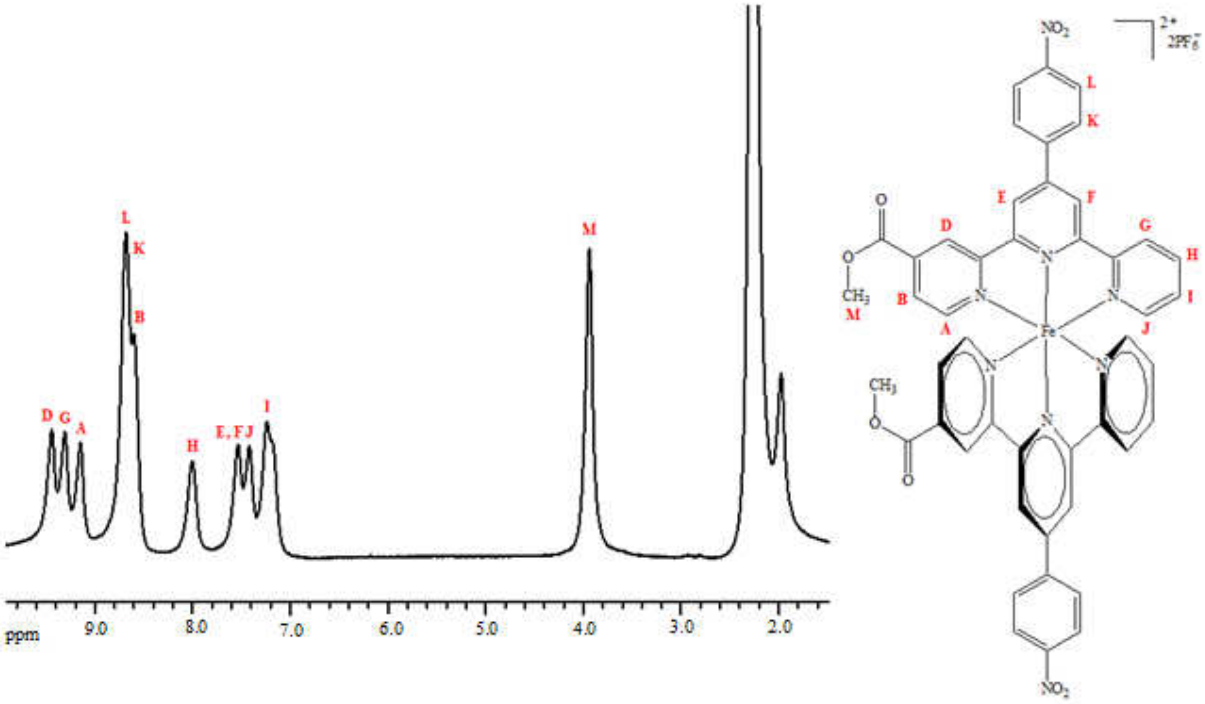

Figure 42. The ^{1}H-NMR spectrum of complex **C2** in CD_3CN.

The ^{13}C-NMR spectrum obtained in CD_3CN was more diagnostic, as it showed all the requisite carbon signals, confirming the low local symmetry.

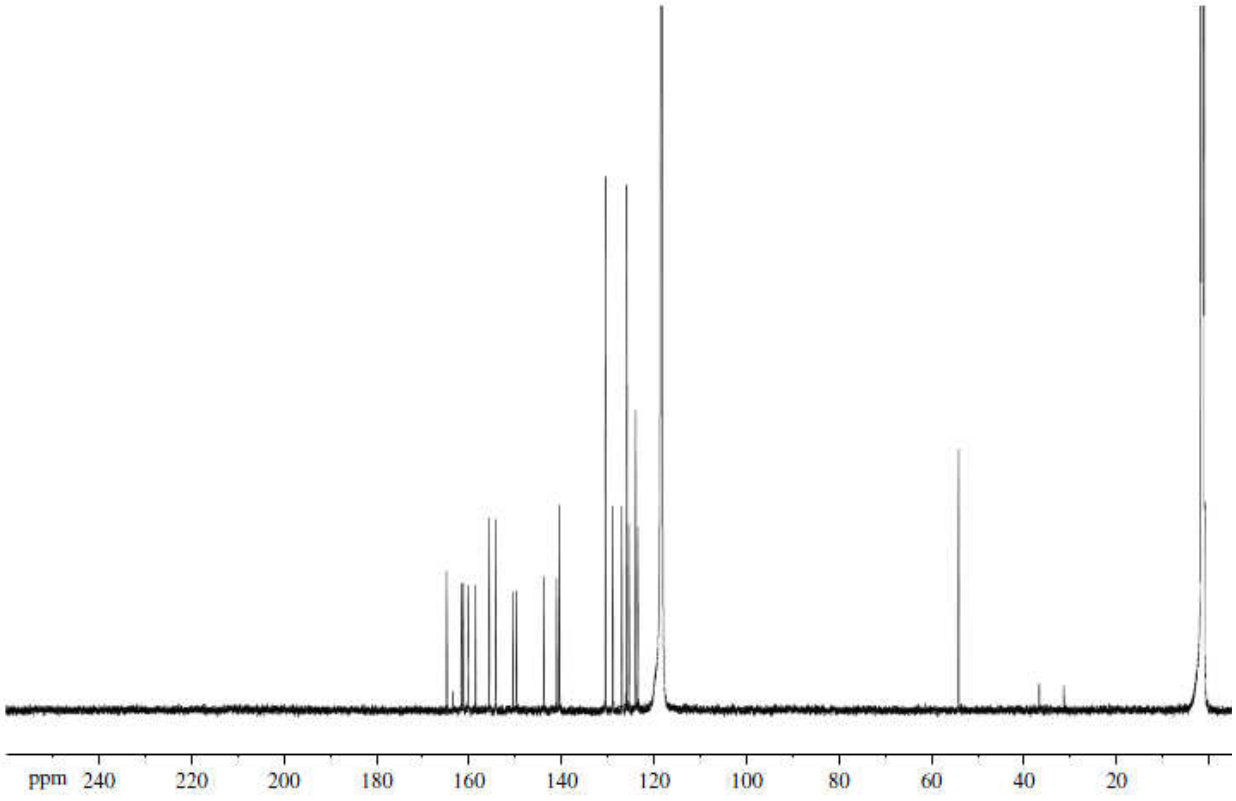

Figure 43. ^{13}C-NMR spectrum of **C2** in CD_3CN.

The IR spectrum is shown below (Figure 44) confirmed the presence of PF_6, as well as carbonyl and nitro stretches.

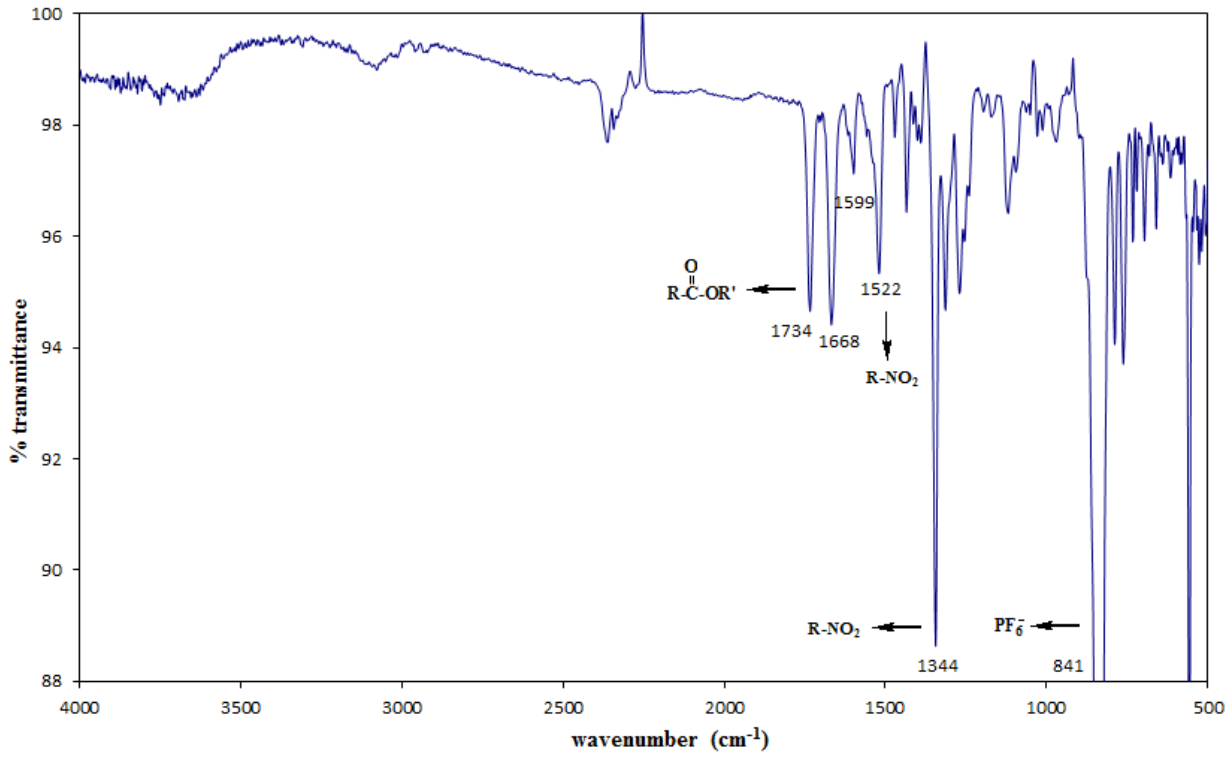

Figure 44. FT-IR spectrum for the complex **C2.**

The ESI-MS spectrum that was obtained for this complex **C2** showed an overlap between two isotopic patterns of two different species, one larger than the other. The experimental spectrum (A) has some extra peaks when compared to the calculated spectrum (B). These peaks correspond to the dimer complex of twice the size and twice the charge (half the peak-to-peak separation) (C). The experimental spectrum and the calculated spectra are shown below (Figure 45).

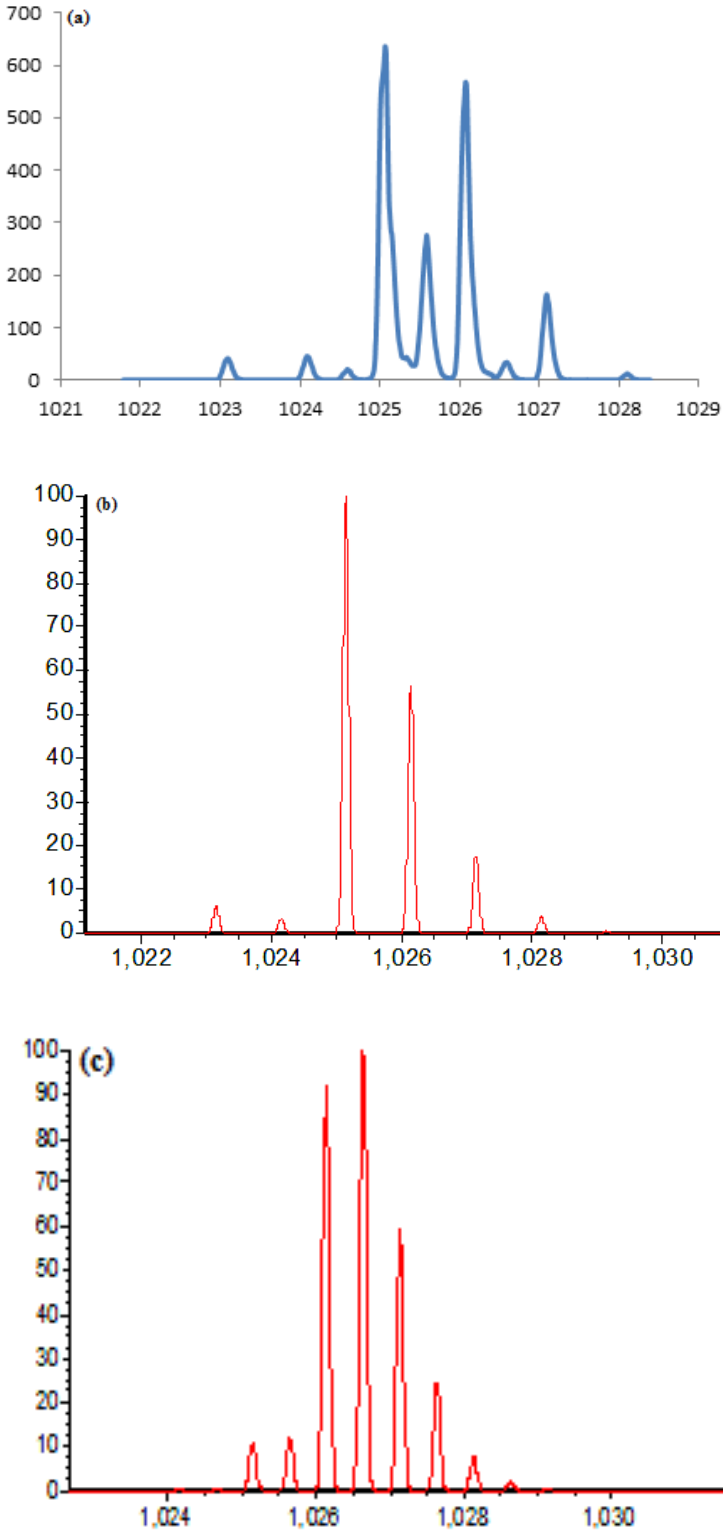

Figure 45. Mass spectrum of **C2** in CH_3CN**:**

top, experimental, and middle, calculated for **C2**; bottom, calculated for the dimer.

The proposed structure of the dimer complex is shown below in Figure 46. This would result from a small amount of ligand scrambling in which one of the terminal pyridines from one of the terpyridine units becomes a unidentate ligand for a second iron. That means that one pyridine falls off, and then the two such molecules pair up together. This represents a simple dimerization, most simply being described by the following equation.

$$2\ [Fe(\mathbf{L4})_2]^{2+} \rightarrow [Fe(\mathbf{L4})_2]_2^{4+}$$

This simple dimerization of the two regular complexes to forming the dimer of double charge has the same mass to charge ratio, but the isotope variants in the dimer species differ by half the m/z value (0.25 amu). This helps us distinguish between those two complexes.

Since there is absolutely no evidence for the formation of this dimer complex by NMR or any other means, a possible explanation for the detection of this dimer in the mass spectrum is that it is an artifact of the sampling in electrospray ionization. As the concentration within the droplet increases due to solvent evaporation, the equilibrium between monomer and dimer is shifted towards the dimer. There was no evidence that this happened with the other iron complex (see below).

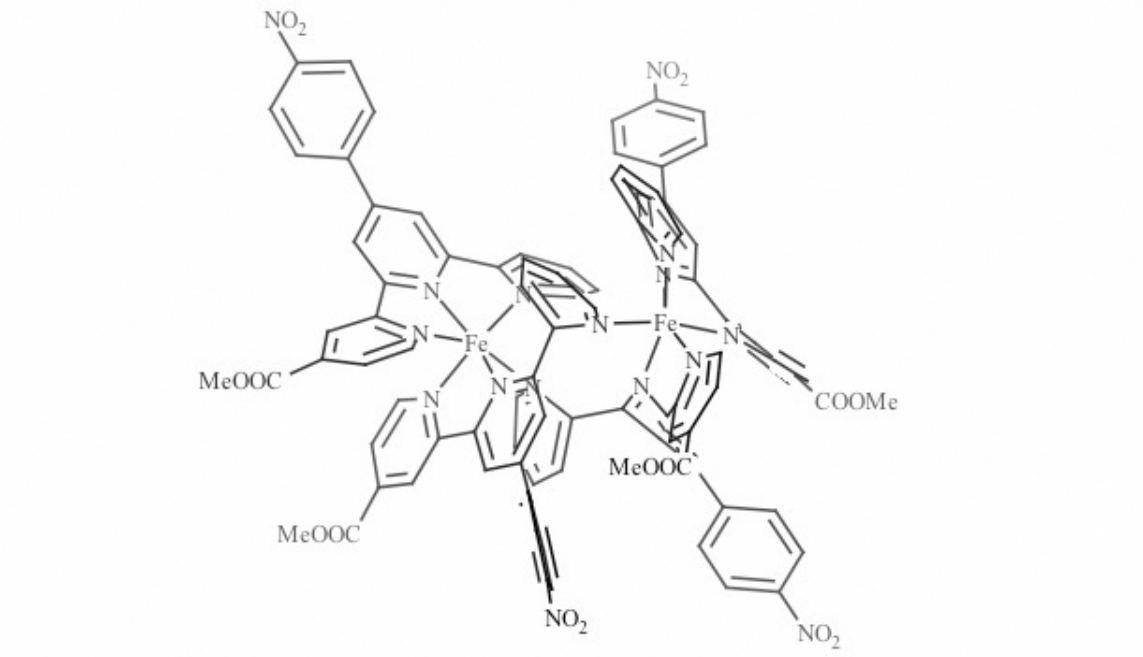

Figure 46. The structure of the proposed dimer complex $[Fe_2(\mathbf{L4})_2(PF_6)_4]$.

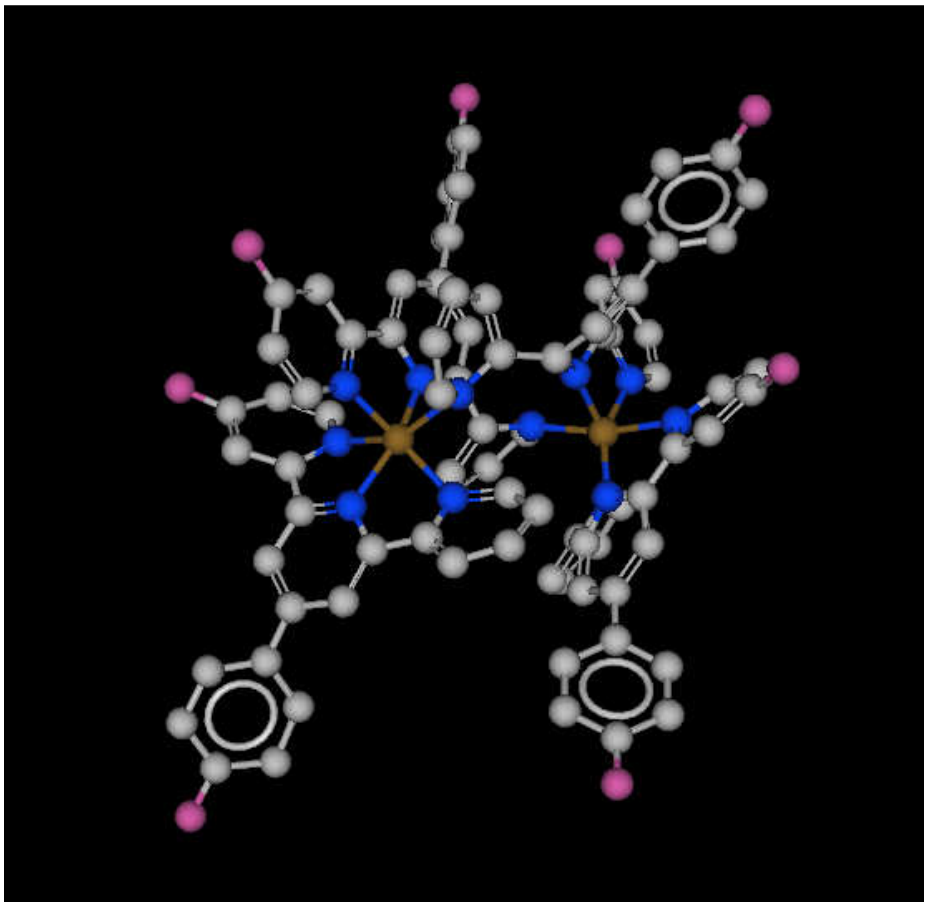

Figure 47. The structure of the proposed dimer complex using the ball and stick model.

3.19. Homoleptic Ru Complex (C3)

We attempted to prepare a homoleptic ruthenium complex from **L5** using the same reaction procedure as for the previous complex. However, the NMR spectrum in the resulting product was not clear, giving only broad signals.

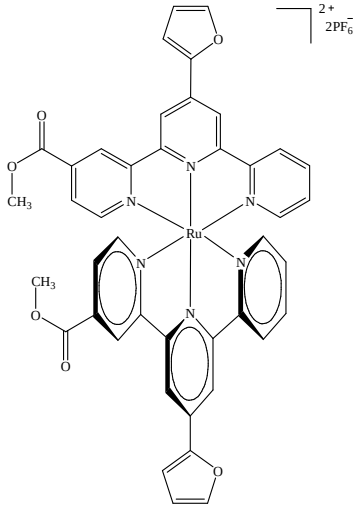

C3

3.20. Homoleptic Fe Complex (C4)

There were several attempts to produce this complex, also beset by solubility issues. Using the same procedure as for **C2**, the overall yield was very high (99%). Again, the ^{1}H-NMR spectra of Figure 49 showed relatively broad signals with a little bit more definition than before, but it was entirely supportive of the structure.

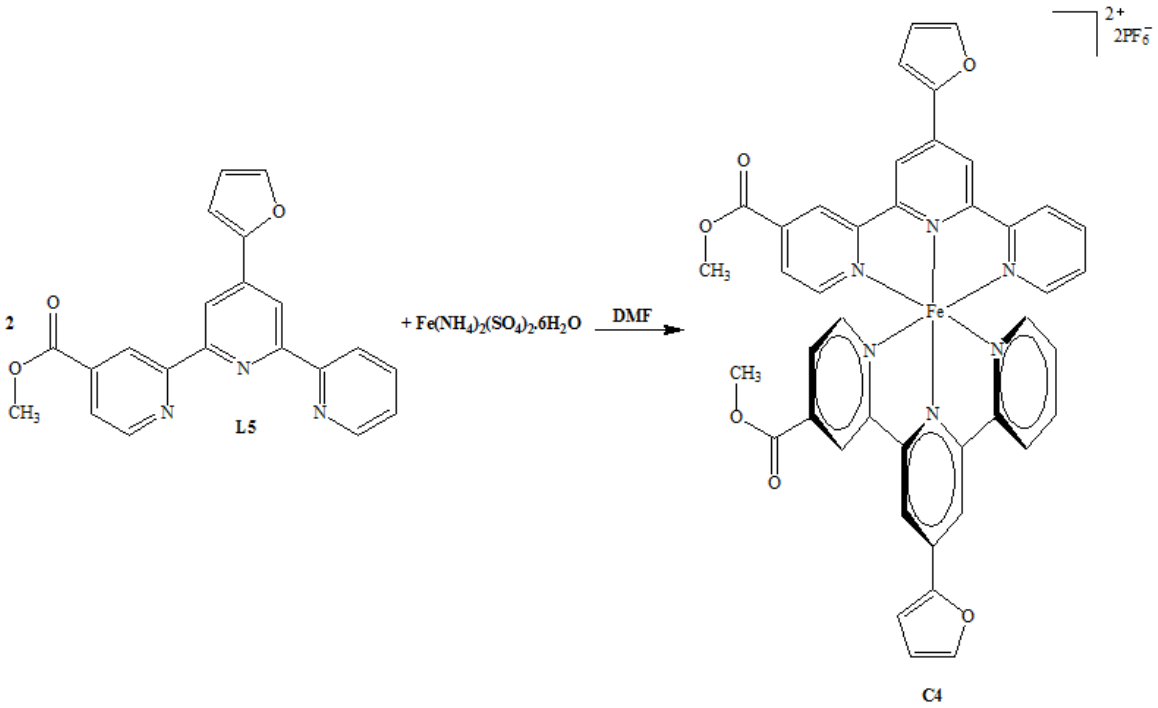

Figure 48. The synthesis of complex **C4**.

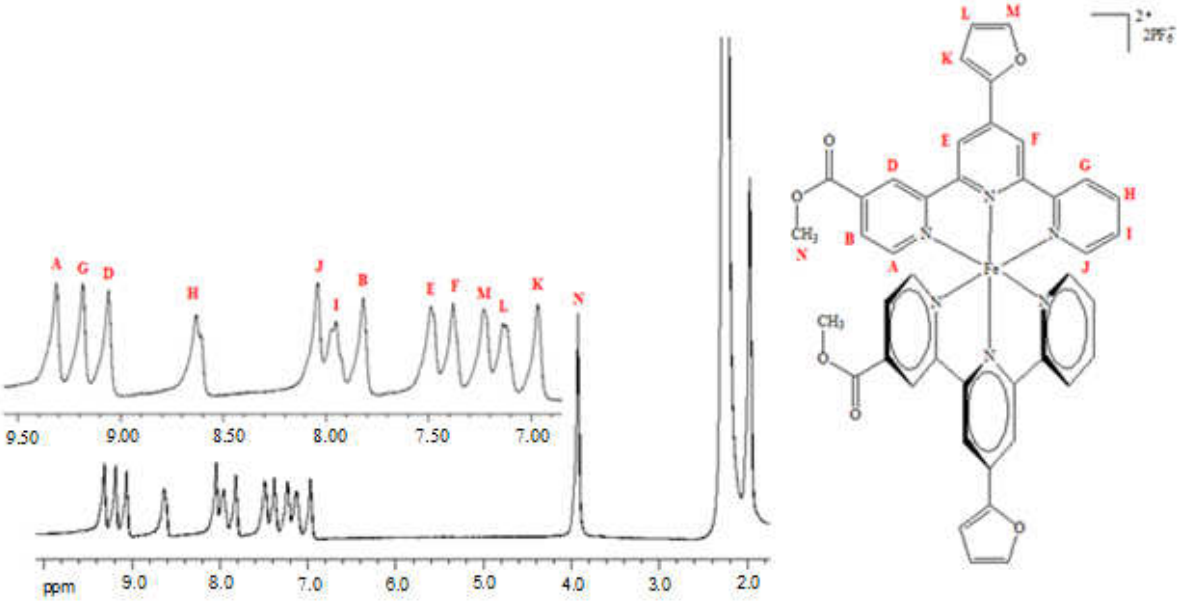

Figure 49. The ^{1}H-NMR spectrum of complex **C4** in CD_3CN.

In addition, the $^{13}C-$NMR spectrum (Figure 50) was obtained in CD_3CN, and it showed all the requisite signals.

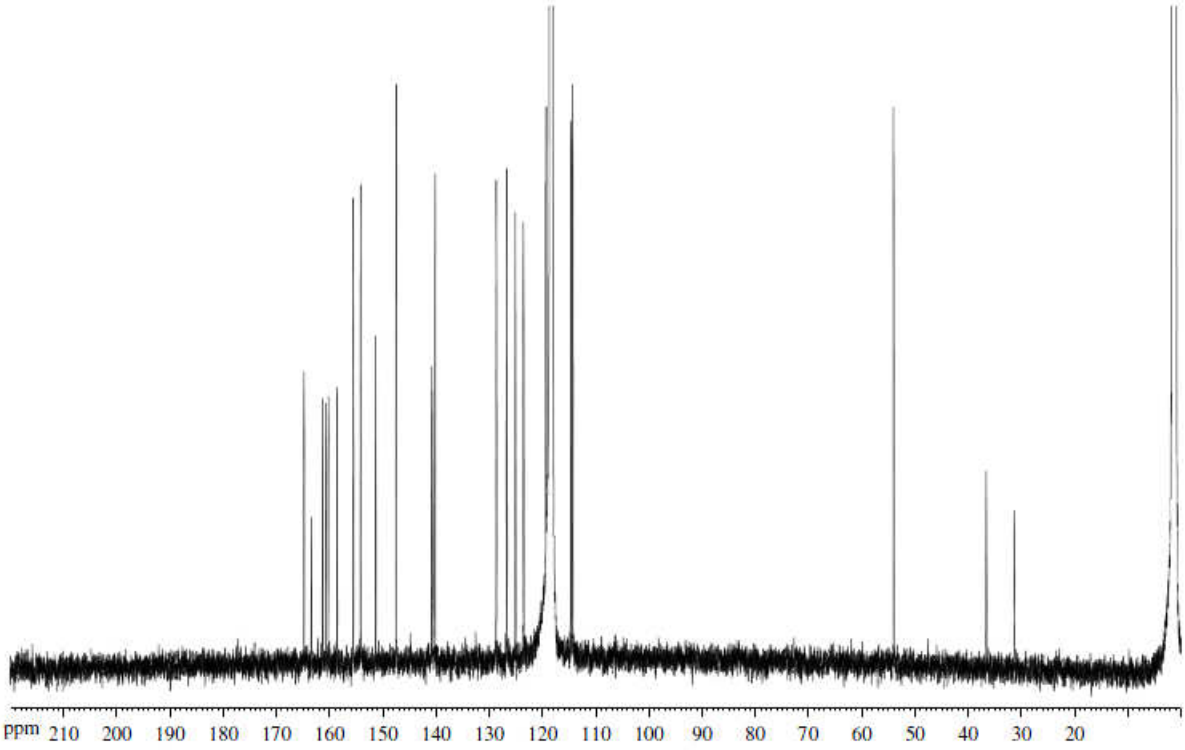

Figure 50. $^{13}C-$NMR spectrum of **C4** in CD_3CN.

The IR spectrum (Figure 51) confirms the presence of PF_6 and also shows the carbonyl stretch.

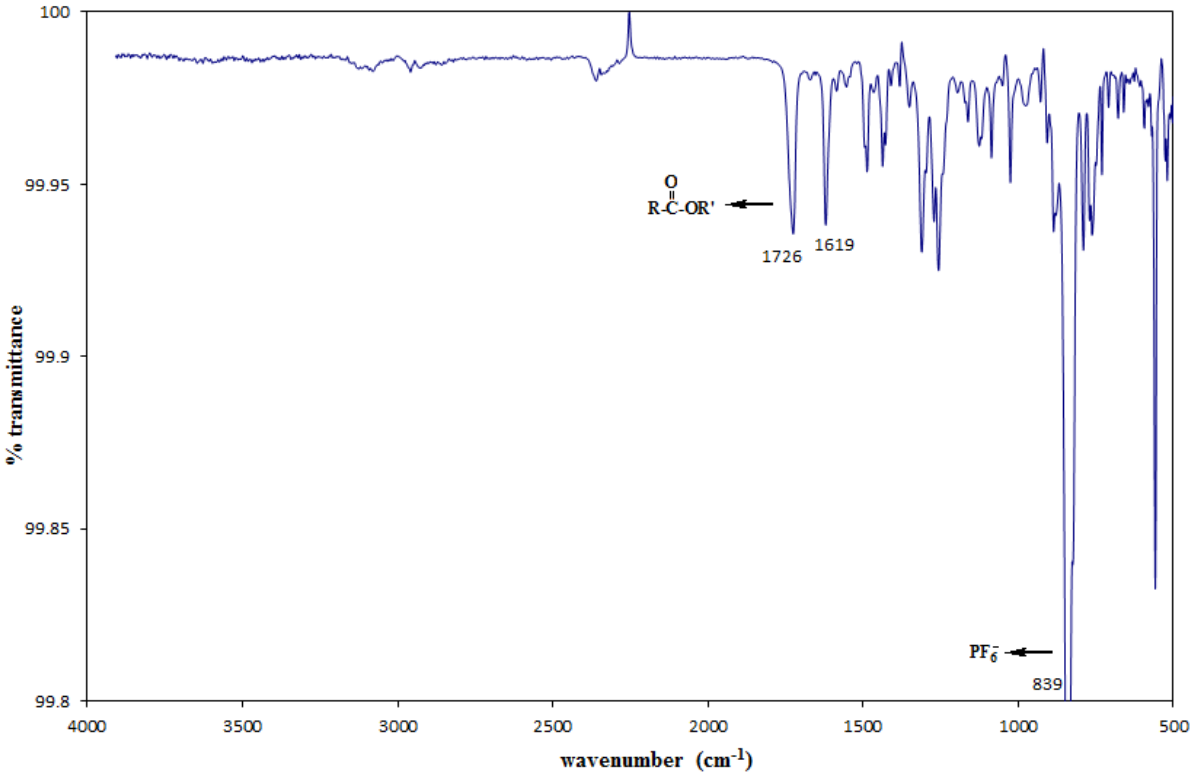

Figure 51. FT-IR spectrum for the complex **C4.**

The ESI-MS spectrum for complex **C4** showed an ion cluster fitting the formula $\{[(\mathbf{C4})_2Fe][PF_6]\}^+$ whose isotopic distribution matched well with that expected for the proposed formula. There was no clear evidence here of the formation of a dimer complex. Hence, the spectrum was fully consistent with the proposed structure.

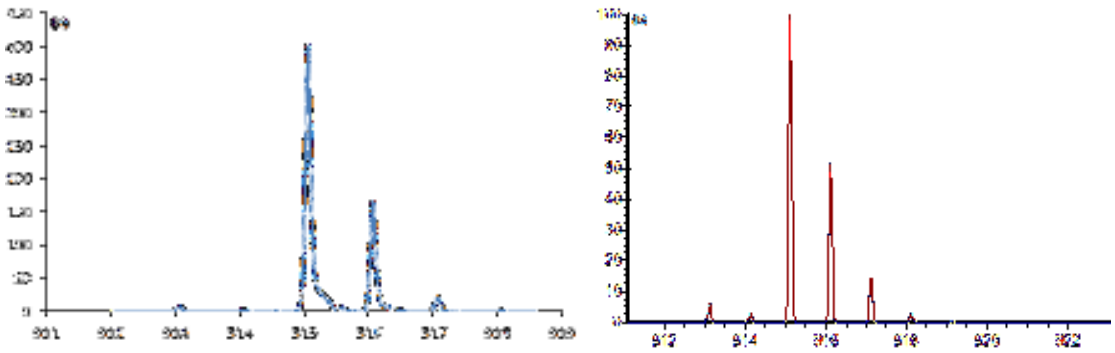

Figure 52. Mass spectrum of **C4** in CH_3CN**:**

at left, experimental; at right, calculated.

The UV-visible analysis of these three complexes is shown below in Figure 53. The spectra showed single MLCT bands at 500 nm for **C1**, 582 nm for **C2**, and a very similar one at 586 nm for **C4**. The spectra are entirely consistent with those of other homoleptic Ru and Fe terpyridine species.

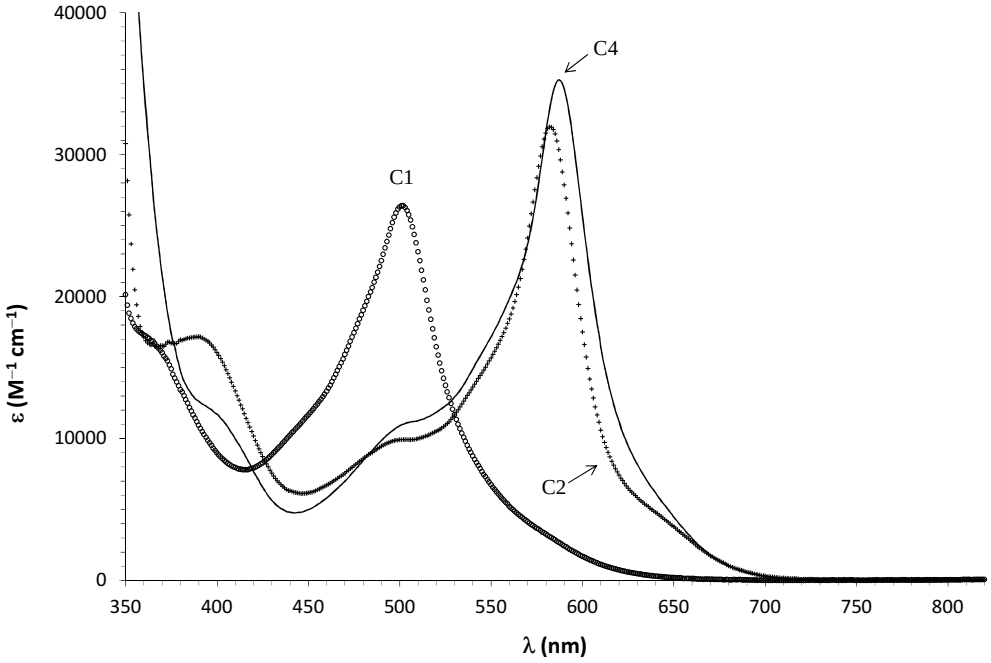

Figure 53. The UV-Visible spectra of the three complexes in CH_3CN.

4.Conclusion & Future Work

There are two mono-4-carboxylated and one 4,4′′-dicarboxylated terpyridine ligands which were prepared with good yields, and the novel homoleptic ruthenium(II) and iron(II) complexes have been synthesized with these ligands with excellent yields. They have been characterized by using ESI-MS, ^{1}H-NMR, ^{13}C-NMR, UV-visible spectroscopy and FT-IR spectroscopy. These characterizations confirm the identity and structural integrity of the prepared complexes.

In the future, these complexes need further characterizations by elemental analysis, as well as COSY NMR, HSQC, HMBC, and perhaps NOESY NMR in order to more completely assign the NMR signals with confidence.

After characterization, these dye complexes will be transformed to carboxylate forms and then transferred over to Prof. Morin's laboratory for absorption onto titanium dioxide plates in the evaluation of the surface properties as well as the photovoltaic performances. Moreover, more work can be done to refine the process by which we could obtain the other enones.

Furthermore, the furan-containing ligand **L5** could be transformed to a dicarboxy species, and the nitrophenyl ligand **L4** could be transformed to the aminophenyl analogue. The aminophenyl variety would give rise then to new homoleptic complexes of ruthenium and iron, and the dicarboxylic form obtained from **L5** could then be used to assemble complexes of type $\mathbf{C_B}$ with MLX_3 formula.

In addition, future work could be done such as electrochemistry in order to be able to characterize the HOMO levels, and we need the emission data to be able to assess LUMO levels and to make sure that LUMO levels are near the conduction band.

5. References

1. Wadman, S., Van Leeuwen, Y., Havenith, R., Van Klink, G. and Van Koten, G. (2010). A Redox Asymmetric, Cyclometalated Ruthenium Dimer: Toward Upconversion Dyes in Dye-Sensitized TiO2 Solar Cells. *Organometallics*, 29 (21), 5635-5645.

2. (a) Hagfeldt, A. and Grätzel, M. (2000). Molecular Photovoltaics. *Accounts of Chemical Research*, 33 (5), 269-277; (b) Lin, J., Chen, J. and Chen, X. (2011). High-efficiency dye-sensitized solar cells based on roubust and both-end-open TiO_2 nanotube membranes. *Nanoscale research letters*, 6 (1), 1-5.

3. Green, M. (2002). Third Generation Photovoltaics: Solar Cells for 2020 and Beyond. *Physica E: Low-Dimensional Systems and Nanostructures*, 14 (1), 65-70.

4. King, R., Bhusari, D., Larrabee, D., Liu, X., Rehder, E., Edmondson, K., Cotal, H., Jones, R., Ermer, J., Fetzer, C. and Others (2012). Solar Cell Generations Over 40% Efficiency. *Progress in Photovoltaics: Research and Applications*, 20 (6), 801-815.

5. Madougou, S., Kaka, M. and Sissoko, G. (2010). Silicon Solar Cells: Recombination and Electrical Parameters. In R. D. Rugescu (Ed.). *Solar Energy* (pp.69-81). Niamey: InTech.

6. Guo, Y., Porter, A. and Huang, L. (2009). Nanotechnology enhanced thin-film solar cells: analysis of global research activities with future prospects. *IAMOT*, 1-17. Retrieved from: https://www.thevantagepoint.com/resources/papers-and-reports/archives-2002-2010/64-nanotechnology-enhanced-t.html [Accessed: 28 Nov 2013].

7. Singh, R., Rangari, V., Sanagapalli, S., Jayaraman, V., Mahendra, S. and Singh, V. (2004). Nano-structured CdTe, CdS and TiO_2 for thin film solar cell applications. *Solar Energy Materials and Solar Cells*, 82 (1), pp. 315-330.

8. Markvart, T. and Castañer, L. (2003). Overview of Potential Hazards. In V. Fthenakis (Ed.). *Practical Handbook of Photovoltaics* (pp. 1-14). New York: Elsevier Advanced Technology.

9. Brown, G. and Wu, J. (2009). Third generation photovoltaics. *Laser & Photonics Reviews*, 3 (4), 394-405.

10. Wei, D. (2010). Dye sensitized solar cells. *International journal of molecular sciences*, 11 (3), 1103-1113.

11. Tian, H., Yu, X., Zhang, J., Duan, W., Tian, F. and Yu, T. (2012). The Influence of Environmental Factors on DSSCs for BIPV. *Int. J. Electrochem. Sci*, 7, 4686-4691.

12. Van Bavel, M., Lutsen, L., Kavan, L., Nazeeruddin, M. and Grätzel, M. (2012). Toward a Novel Generation of Thin Film Dye-Sensitized Solar Cells. *Journal of New Technology and Materials*, 1-3.

13. Wenger, S. (2010). *Strategies to optimizing dye-sensitized solar cells: organic sensitizers, tandem device structures, and numerical device modeling*. [e-book] Suisse: [S.l.]: [s.n.]. pp. 1-165. Available through: google scholar http://infoscience.epfl.ch/record/150259/files/EPFL_TH4805.pdf [Accessed: 26 Nov 2013].

14. Stathatos, E. (2011). Dye Sensitized Solar Cells as an Alternative Approach to the Conventional Photovoltaic Technology Based on Silicon - Recent Developments in the Field and Large Scale Applications. In L. Kosyachenko (Ed.). *Solar Cells - Dye-Sensitized Devices* (pp. 471-492). Patras: InTech.

15. Ito, S. (2011). Investigation of dyes for dye-sensitized solar cells: Ruthenium-complex dyes, metal-free dyes, metal-complex porphyrin dyes and natural dyes. In L. A. Kosyachenko (Ed.). *Solar Cells - Dye-Sensitized Devices* (pp. 19-48). Hyogo: InTech.

16. Chen, Z., Li, F. and Huang, C. (2007). Organic D-π-A Dyes for Dye-Sensitized Solar Cell. *Current Organic Chemistry*, 11 (14), 1241-1258.

17. Lee, E., Jung, N., Kim, J., Im, C., Seo, Y., Hwang, H. and Kang, Y. (2012). Synthesis of Alkyl-functionalized Organic Dyes and Their Application to Dye Sensitized Solar Cells (DSSCs). *Notes*, 33 (1), 293-296.

18. Jiao, Y., Zhang, F., Meng, S. (2011). Dye Sensitized Solar Cells Principles and New Design. In L. A. Kosyachenko (Ed.). *Solar Cells - Dye-Sensitized Device* (pp. 131-148). Beijing: InTech.

19. Zen, S., Teramoto, Y., Hanawa, K., Kobayashi, S., Ono, R. and Oda, T. (2012). Surface treatment of dye-sensitized solar cell using dielectric barrier discharge. *Proc*.1-6. Retrieved from: ttp://www.electrostatics.org/images/ESA2012_B3.pdf [Accessed: 28 Nov 2013].

20. Grätzel, M., and Durrant, J. (1912). *Dye-Sensitised Mesoscopic Solar Cells (Chapter8),* Washington and New York: Imperial College Press.

21. Chou, T., Zhang, Q., Russo, B. and Cao, G. (2008). Enhanced light-conversion efficiency of titaniumdioxide dye-sensitized solar cells with the addition of indium-tin-oxide and fluorine-tin-oxide nanoparticles in electrode films. *Journal of Nanophotonics*, 2 (023511), 1-11.

22. Grätzel, M. (2003). Dye-sensitized solar cells. *Journal of Photochemistry and Photobiology C: Photochemistry Reviews*, 4 (2), 145-153.

23. Smith, W., Mao, S., Lu, G., Catlett, A., Chen, J. and Zhao, Y. (2010). The effect of Ag nanoparticle loading on the photocatalytic activity of TiO_2 nanorod arrays. *Chemical Physics Letters*, 485 (1), 171-175.

24. Devi, K., Sreeja, P. and Sugunan, S. (2013). Environmentally benign Friedel-Crafts benzylation over nano-TiO_2/SO_4^{2-}. *International Nano Letters*, 3 (1), 40.

25. Wang, D., Choi, D., Yang, Z., Viswanathan, V., Nie, Z., Wang, C., Song, Y., Zhang, J. and Liu, J. (2008). Synthesis and Li-ion insertion properties of highly crystalline mesoporous rutile TiO_2. *Chemistry of Materials*, 20 (10), 3435-3442.

26. Jensen, H., Gibson, U. and Cui, J. (2006). ZnO and TiO_2 dye-sensitized Graetzel cells.

27. Heitjans, P. and Indris, S. (2003). Diffusion and ionic conduction in nanocrystalline ceramics. *Journal of Physics: Condensed Matter*, 15 (30), 1257.

28. Wang, H., Su, C., Chen, H., Liu, Y., Hsu, Y., Hsu, N. and Li, W. (2011). Preparation of Nanoporous TiO_2 Electrodes for Dye-Sensitized Solar Cells. *Journal of Nanomaterials*, 2011 (547103), 7.

29. Park, N., Van De Lagemaat, J. and Frank, A. (2000). Comparison of dye-sensitized rutile-and anatase-based TiO_2 solar cells. *The Journal of Physical Chemistry B*, 104 (38), 8989-8994.

30. Hwang, K., Yoo, S., Kim, S., Kim, J., Shim, W., Kim, S. and Lee, J. (2008). Photovoltaic Performance of Nanoporous TiO_2 Replicas Synthesized from Mesoporous Materials for Dye-Sensitized Solar Cells. *Journal of Nanoscience and Nanotechnology*, 8 (10), 4976-4981.

31. Stathatos, E. and Dionysiou, D. (n.d.). Comparative studies on Dye Sensitized Solar Cells with nanostructured TiO_2 films prepared in room or in high temperature. *Yumpu*, 1-5.

32. Yorku.ca (2013). *pgpotvin@chem.yorku.ca*. [online] Retrieved from: http://www.yorku.ca/pgpotvin/projects.htm#1 [Accessed: 13 Nov 2013].

33. Sokolský, M. and Cirák, J. (2010). Dye-Sensitized Solar Cells: Materials and Processes. *Acta Electrotechnica et Informatica*, 10 (3), 78-81.

34. Desilvestro, H. and Hebting, Y. (n.d.). *Ruthenium-based dyes for Dye Solar Cells*. [online] Retrieved from: http://www.sigmaaldrich.com/materials-science/organic-electronics/dye-solar-cells.html [Accessed: 13 Nov 2013].

35. Katz, J. (2008). Metal oxide-based photoelectrochemical cells for solar energy conversion (Doctoral dissertation, California Institute of Technology). Retrieved from http://thesis.library.caltech.edu/4186/1/Jordan_Katz_Thesis2007.pdf

36. Lee, C., Chen, P. & Ho, K. (2011). Ionic Liquid Based Electrolytes for Dye-Sensitized Solar Cells. In: A. Kokorin (Ed.). *Ionic Liquids: Theory, Properties, New Approaches (*pp. 631-656). Rijeka: InTech.

37. Wu, J., Lan, Z., Hao, S., Li, P., Lin, J., Huang, M., Fang, L., Huang, Y. and Others (2008). Progress on the electrolytes for dye-sensitized solar cells. *Pure and Applied Chemistry*, 80 (11), 2241-2258.

38. Feldt, S. 2013. Alternative Redox Couples for Dye-Sensitized Solar Cells. Acta Universitatis Upsaliensis. *Digital Comprehensive Summaries of Uppsala Dissertations from the Faculty of Science and Technology* 1017. 1-80. Uppsala. ISBN 978-91-554-8595-5.

39. Wang, M., Chamberl, N., Breau, L., Moser, J., Humphry-Baker, R., Marsan, B., Zakeeruddin, S. and Grätzel, M. (2010). An organic redox electrolyte to rival triiodide/iodide in dye-sensitized solar cells. *Nature Chemistry*, 2 (5), 385-389.

40. Yum, J., Baranoff, E., Kessler, F., Moehl, T., Ahmad, S., Bessho, T., Marchioro, A., Ghadiri, E., Moser, J., Yi, C. and Others (2012). A Cobalt Complex Redox Shuttle For Dye-Sensitized Solar Cells with High Open-Circuit Potentials. *Nature Communications*, 3, 631.

41. Pursel, S. (2011). Dye Sensitized Solar Cells Based on Nanowire Sculptured Thin Film Titanium Dioxide Photoanodes (Doctoral dissertation, The Pennsylvania State University). Retrieved from https://www.google.ca/url?sa=t&rct=j&q=&esrc=s&source=web&cd=1&ved=0CC0QFjAA&url=https%3A%2F%2Fetda.libraries.psu.edu%2Fpaper%2F12038%2F8218&ei=aa5oUq-FIOaC2wXb04B4&usg=AFQjCNEjSwMXeTz6VWhOJivmuL1gpUBLg&sig2=4cRDo7UHunrB9Qe1uY4OKw&bvm=bv.55123115,d.b2I&cad=rt

42. Hardin, B., Snaith, H. and Mcgehee, M. (2012). The renaissance of dye-sensitized solar cells. *Nature Photonics*, 6 (3), 162-169.

43. Murakami, T. and Koumura, N. (2013). Performance enhancement of dye-sensitized solar cells with organic dyes. *IEEE Xplore,* 83-86.

44. Yu, Z. (2012). Liquid Redox Electrolytes for Dye-Sensitized Solar Cells (Doctoral dissertation, KTH Chemical Science and Engineering, Royal Institute of Technology). Retrieved from http://www.diva-portal.org/smash/get/diva2:483008/FULLTEXT01.pdf

45. Daeneke, T., Kwon, T., Holmes, A., Duffy, N., Bach, U. and Spiccia, L. (2011). High-efficiency dye-sensitized solar cells with ferrocene-based electrolytes. *Nature Chemistry*, 3 (3), 211-215.

46. Soo-Jin, M. (2011). Solid-State Sensitized Heterojunction Solar Cells: Effect of Sensitizing Systems on Performance and Stability (thesis,The École polytechnique fédérale de Lausanne EPFL). Retrieved from http://infoscience.epfl.ch/record/162123.

47. Nath, N., Kim, J., Kim, K., Yim, S. and Lee, J. (2013). Deprotonation of N3 adsorbed on TiO_2 for high-performance dye-sensitized solar cells (DSSCs). *Journal of Materials Chemistry A*, 1 (43), 13439-13442.

48. Jasim, K. E. (2011). Dye sensitized solar cells - working principles, challenges and opportunities. In L. A. Kosyachenko (Ed.). *Solar Cells - Dye-Sensitized Devices* (pp. 172-204). Kingdom of Bahrain: InTech.

49. Qin, Y. and Peng, Q. (2012). Ruthenium Sensitizers and Their Applications in Dye-Sensitized Solar Cells. *International Journal of Photoenergy*, 2012, 21.

50. Hamann, T., Jensen, R., Martinson, A., Van Ryswyk, H. and Hupp, J. (2008). Advancing beyond current generation dye-sensitized solar cells. *Energy & Environmental Science*, 1 (1), 66-78.

51. Wu, J., Lan, Z., Hao, S., Li, P., Lin, J., Huang, M., Fang, L., Huang, Y. and Others (2008). Progress on the electrolytes for dye-sensitized solar cells. *Pure and Applied Chemistry*, 80 (11), 2241-2258.

52. Pootrakulchote, N. (2012). Investigation on Functionalized Ruthenium-Based Sensitizers to Enhance Performance and Robustness of Dye-Sensitized Solar Cells (thesis, The École polytechnique fédérale de Lausanne EPFL). Retrieved from http://infoscience.epfl.ch/record/177327.

53. Sigma-Aldrich (2013). *Organic Dyes for Efficient and Stable Dye-Sensitized Solar Cells*. [online] Retrieved from: http://www.sigmaaldrich.com/technical-

documents/articles/material-matters/organic-dyes-for-efficient.html [Accessed: 26 Nov 2013].

54. Hara, K., Sato, T., Katoh, R., Furube, A., Ohga, Y., Shinpo, A., Suga, S., Sayama, K., Sugihara, H. and Arakawa, H. (2003). Molecular design of coumarin dyes for efficient dye-sensitized solar cells. *The Journal of Physical Chemistry B*, 107 (2), 597-606.

55. Boschloo, G. and Hagfeldt, A. (2009). Characteristics of the iodide/triiodide redox mediator in dye-sensitized solar cells. *Accounts of chemical research*, 42 (11), 1819-1826.

56. Lee, Y. and Kang, M. (2010). The optical properties of nanoporous structured titanium dioxide and the photovoltaic efficiency on DSSC. *Materials Chemistry and Physics*, 122 (1), 284-289.

57. Ma, Y. (2013). Pore-size Dependence of Ion Diffusivity in Dye-sensitized Solar Cells(Thesis, McMaster University). Retrieved from http://digitalcommons.mcmaster.ca/cgi/viewcontent.cgi?article=8820&context=opendissertations

58. Kolemen, S., Cakmak, Y., Erten-Ela, S., Altay, Y., Brendel, J., Thelakkat, M. and Akkaya, E. (2010). Solid-state dye-sensitized solar cells using red and near-IR absorbing bodipy sensitizers. *Org. Lett*, 12 (17), 3812-3815.

59. Goddard, V. (2006). The synthesis and application of near infrared absorbing dyes in photoelectrochemical cells (Thesis, Queensland University of Technology). Retrieved from http://eprints.qut.edu.au/16272/1/Victoria_Goddard_Thesis.pdf

60. Lee, C. P., Chen, P. Y. & Ho, K. C. (2011). Ionic liquid based electrolytes for dye-sensitized solar cells. In A.Kokorin (Ed.). *Ionic liquids: Theory, properties, new approaches* (pp. 631-656). Rijeka: InTech.

61. Havaux, M. and Tardy, F. (1997). Thermostability and photostability of photosystem II in leaves of the Chlorina-f2 barley mutant deficient in light-harvesting chlorophyll a/b protein complexes. *Plant physiology*, 113 (3), 913-923.

62. Xue, G., Guo, Y., Yu, T., Guan, J., Yu, X., Zhang, J., Liu, J. and Zou, Z. (2012). Degradation mechanisms investigation for long-term thermal stability of dye-sensitized solar cells. *Int. J. Electrochem. Sci*. 7, 1496-1511.

63. Hara, K. and Arakawa, H. (2005). Dye-Sensitized Solar Cells. In A. Luque and S. Hegedus (Eds.). *Handbook of Photovoltaic Science and Engineering* (pp. 663-700). Chichester: John Wiley & Sons, Ltd.

64. Cai, S., Tian, G., Li, X., Su, J. and Tian, H. (2013). Efficient and stable DSSC sensitizers based on substituted dihydroindolo [2, 3-b] carbazole donors with high molar extinction coefficients. *J. Mater. Chem. A*, 1 (37), 11295-11305.

65. Delgado, J., Zhang, Y., Xu, B. and Epstein, I. (2011). Terpyridine-and Bipyridine-Based Ruthenium Complexes as Catalysts for the Belousov- Zhabotinsky Reaction. *The Journal of Physical Chemistry A*, 115 (11), 2208-2215.

66. Beck, J., Humphries, A., Sheil, M. and Ralph, S. (1999). Electrospray ionisation mass spectrometry of ruthenium and palladium complexes with oligonucleotides. *European Journal of Mass Spectrometry (EJMS).* 5, 489-500.

67. Nurkkala, L. (2007). Design, Synthesis and Properties of Bipyridine-capped Oligothiophenes for Directed Energy and Electron Transfer in Molecular Electronic

Applications (Doctoral dissertation, Mälardalen University). Retrieved from http://www.diva-portal.org/smash/record.jsf?pid=diva2:120974

68. (a) Fantacci, S., De Angelis, F. and Selloni, A. (2003). Absorption spectrum and solvatochromism of the [Ru (4, 4'-COOH-2, 2'-bpy)$_2$ (NCS)$_2$] molecular dye by time dependent density functional theory. *Journal of the American Chemical Society*, 125 (14), 4381-4387; (b) Brewster, T. P., Ding, W., Schley, N. D., Hazari, N., Batista, V. S. and Crabtree, R. H. 2011. Thiocyanate Linkage Isomerism in a Ruthenium Polypyridyl Complex. Inorganic Chemistry, 50 (23), 11938-11946.

69. Menting, R. (2013). Light-induced energy and charge transfer processes in artificial photosynthetic systems (Thesis, Humboldt University). Retrieved from http://www.mysciencework.com/publication/show/87047/light-induced-energy-and-charge-transfer-processes-in-artificial-photosynthetic-systems-light-induced-energy-and-charge-transfer

70. Griffith, M. J. & Mozer, A. J. (2011). Porphyrin based dye sensitized solar cells. In L. A. Kosyachenko (Ed.). *Solar Cells -Dye-Sensitized Devices* (pp. 374-398). Fairy Meadow: InTech.

71. Nazeeruddin, M., Péchy, P., Renouard, T., Zakeeruddin, S., Humphry-Baker, R., Comte, P., Liska, P., Cevey, L., Costa, E., Shklover, V., Spiccia, L., Deacon, G., Bignozzi, C., and Grätzel, M. (2001). Engineering of efficient panchromatic sensitizers for nanocrystalline TiO_2-based solar cells. *Journal of the American Chemical Society*, *123* (8), 1613-1624.

72. Daeneke, T., Mozer, A., Kwon, T., Duffy, N., Holmes, A., Bach, U. and Spiccia, L. (2012). Dye regeneration and charge recombination in dye-sensitized solar cells with

ferrocene derivatives as redox mediators. *Energy & Environmental Science*, 5 (5), 7090-7099.

73. Wang, H., Liu, M., Zhang, M., Wang, P., Miura, H., Cheng, Y. and Bell, J. (2011). Kinetics of electron recombination of dye-sensitized solar cells based on TiO_2 nanorod arrays sensitized with different dyes. *Physical Chemistry Chemical Physics*, 13 (38), 17359-17366.

74. (a) Sekar, N. and Gehlot, V. (2010). Metal complex dyes for dye-sensitized solar cells: Recent developments. *Resonance*, 15 (9), 819; (b) Ryan, M. (2009). Progress in Ruthenium Complexes for Dye Sensitised Solar Cells. In *Platinum Metals Rev*,*53*(4). Retrieved December 30, 2013 from http://www.platinummetalsreview.com/article/53/4/216-218/#references

75. (a) Jamula, L. L. (2010). Design and synthesis of iron (II) terpyridyl complexes for application in dye-sensitized solar cells (Thesis, Michigan State University). Retrieved from http://search.proquest.com.ezproxy.library.yorku.ca/docview/815243224?accountid=15182. (815243224); (b) Hagberg, D. (2009). Synthesis of Organic Chromophores for Dye Sensitized Solar Cells (Doctoral dissertation, Royal Institute of Technology). Retrieved from http://www.diva-portal.org/smash/get/diva2:219044/FULLTEXT01

76. Sharma, G., Singh, S., Kurchania, R. and Ball, R. (2013). Cosensitization of dye sensitized solar cells with a thiocyanate free Ru dye and a metal free dye containing thienylfluorene conjugation. *RSC Adv.*, 3 (17), 6036-6043.

77. Wang, S., Wu, K., Ghadiri, E., Lobello, M., Ho, S., Chi, Y., Moser, J., De Angelis, F., Gr\"Atzel, M. & Nazeeruddin, M. (2013). Engineering of thiocyanate-free Ru(II) sensitizers for high efficiency dye-sensitized solar cells. *Chem. Sci.*, *4* (6), 2423-2433.

78. Ferrere, S. (n.d.). Untitled. *Development of new dyes for the dye sensitized solar cell*, Retrieved from: http://www.electrochem.org/dl/ma/199/pdfs/0614.pdf [Accessed: 15 Nov 2013].

79. Meyer, G. (2005). Molecular approaches to solar energy conversion with coordination compounds anchored to semiconductor surfaces. *Inorganic chemistry*, 44 (20), 6852-6864.

80. Ferrere, S. (2000). New photosensitizers based upon $[Fe(L)_2\ (CN)_2]$ and $[Fe(L)_3]$(L= substituted 2, 2'-bipyridine): Yields for the photosensitization of TiO_2 and effects on the band selectivity. *Chemistry of materials*, 12 (4), 1083-1089.

81. Lu, X., Wei, S., Wu, C., Ding, N., Li, S., Zhao, L. and Guo, W. (2011). Theoretical Insight into the Spectral Characteristics of Fe(II)-Based Complexes for Dye-Sensitized Solar Cells-Part I: Polypyridyl Ancillary Ligands. *International Journal of Photoenergy*, 2011, 11.

82. Giribabu, L., Sudhakar, K. and Velkannan, V. (2012). Phthalocyanines: potential alternative sensitizers to Ru (II) polypyridyl complexes for dye-sensitized solar cells. *Current Science(Bangalore)*, 102 (7), 991-1000.

83. Chamchoumis, C. and Potvin, P. (1998). Condensation Reactions of 2-Acetylpyridine and Benzaldehydes: New Cyclohexanol Products and an Improved Synthesis of 4′-p-Tolyl-2, 2′: 6′, 2 ″-terpyridine. *Journal of Chemical Research, Synopses*, (4), 180-181.

84. Mukkala, V., Helenius, M., Hemmil\"A, I., Kankare, J. and Takalo, H. (1993). Development of luminescent europium(III) and terbium(III) chelates of 2, 2′: 6′, 2 ″-terpyridine derivatives for protein labelling. *Helvetica chimica acta*, 76 (3), 1361-1378.

85. Wadman, S., Kroon, J., Bakker, K., Havenith, R., Van Klink, G. and Van Koten, G. (2010). Cyclometalated organoruthenium complexes for application in dye-sensitized solar cells. *Organometallics*, 29 (7), 1569-1579.

86. Mikel, C. and Potvin, P. (2002). Synthesis and enhanced photosensitization ability of a 4-carboxy-2, 2′: 6′, 2′′-terpyridine complex of ruthenium(II). *Polyhedron*, 21 (1), 49-54.

87. Masciello, L. and Potvin, P. (2003). One-pot synthesis of terpyridines and macrocyclization to C3-symmetric cyclosexipyridines. *Canadian journal of chemistry*, 81 (3), 209-218.

88. Tran, T., Nguyen, T., Do, T., Huynh, T., Tran, C., Thai, K. and Others (2012). Synthesis and Antibacterial Activity of Some Heterocyclic Chalcone Analogues Alone and in Combination with Antibiotics. *Molecules*, 17 (6), 6684-6696.

89. Montes-Avila, J., Diaz-Camacho, S., Sicairos-Félix, J., Delgado-Vargas, F. and Rivero, I. (2009). Solution-phase parallel synthesis of substituted chalcones and their antiparasitary activity against Giardia lamblia. *Bioorganic & medicinal chemistry*, 17 (18), 6780-6785.

90. Mukkala, V., Helenius, M., Hemmila, I., Kankare, J. and Takalo, H. (1993). Development of luminescent europium(III) and terbium(III) chelates of 2, 2′: 6′, 2 ″-terpyridine derivatives for protein labelling. *Helvetica chimica acta*, 76 (3), 1361-1378.

91. Zhao, L., Kim, T., Ahn, S., Kim, T., Kim, E., Cho, W., Choi, H., Lee, C., Kim, J., Jeong, T., Chang, C. and Lee, E. (2001). Synthesis, topoisomerase I inhibition and antitumor cytotoxicity of 2,2′:6′,2″-, 2,2′:6′,3″- and 2,2′:6′,4″-Terpyridine derivatives.

ScienceDirect, 11 (19), 2659–2662. Retrieved from: http://www.sciencedirect.com/science/article/pii/S0960894X01005315# [Accessed: 25 Nov 2013].

92. Merino, P., Franco, S., Merchan, F. and Tejero, T. (1998). Nucleophilic Additions of 2-Furyllithium to Carbonyl Derivatives of L-Serine. Formal Synthesis of (2R, 3R) -b-Hydroxy Aspartic Acid. *Molecules*, 3 (1), 26-30.

93. Wang, J. and Hanan, G. 2005. A Facile Route to Sterically Hindered and Non-Hindered 4′-Aryl-2, 2′: 6′, 2′′-Terpyridines.*Synlett*, 2005 (08), 1251-1254.

94. Constable, E., Dunphy, E., Housecroft, C., Neuburger, M., Schaffner, S., Schaper, F. and Batten, S. (2007). Expanded ligands: bis (2, 2′: 6′, 2 ″-terpyridine carboxylic acid) ruthenium(ii) complexes as metallosupramolecular analogues of dicarboxylic acids. *Dalton Transactions*, (38), 4323-4332.

95. Husson, J. and Knorr, M. (2012). Syntheses and applications of furanyl-functionalized 2,2':6',2''-terpyridines. *Beilstein Journal of Organic Chemistry, 8,* 379-389. Retrieved from: http://www.unboundmedicine.com/medline/citation/22509206/Syntheses_and_applications_of_furanyl_functionalised_22%27:6%272%27%27_terpyridines_.